Steel and Composite Structures, *Vol. 46, No. 3 (2023) 293-318*
https://doi.org/10.12989/scs.2023.46.3.293

Determining elastic lateral stiffness of steel moment frame equipped with elliptic brace

Habib Ghasemi Jouneghani*[1], Nader Fanaie[2a], Mohammad Talebi Kalaleh[3b] and Mina Mortazavi[1c]

[1]*School of Civil and Environmental Engineering, University of Technology Sydney, NSW, Australia*
[2]*Department of Civil Engineering, K. N. Toosi University of Technology, Tehran, Iran*
[3]*Department of Civil and Environmental Engineering, University of Alberta, Canada*

(Received March 23, 2022, Revised December 4, 2022, Accepted January 2, 2023)

Abstract. This study aims to examine the elastic stiffness properties of Elliptic-Braced Moment Resisting Frame (EBMRF) subjected to lateral loads. Installing the elliptic brace in the middle span of the frames in the facade of a building, as a new lateral bracing system not only it can improve the structural behavior, but it provides sufficient space to consider opening it needed. In this regard, for the first time, an accurate theoretical formulation has been developed in order that the elastic stiffness is investigated in a two-dimensional single-story single-span EBMRF. The concept of strain energy and Castigliano's theorem were employed to perform the analysis. All influential factors were considered, including axial and shearing loads in addition to the bending moment in the elliptic brace. At the end of the analysis, the elastic lateral stiffness could be calculated using an improved relation through strain energy method based on geometric properties of the employed sections as well as specifications of the utilized materials. For the ease of finite element (FE) modeling and its use in linear design, an equivalent element was developed for the elliptic brace. The proposed relation was verified by different examples using OpenSees software. It was found that there is a negligible difference between elastic stiffness values derived by the developed equations and those of numerical analysis using FE method.

Keywords: Castigliano's theorem; drift; elastic lateral stiffness; elliptic-braced moment frame; Numerical analysis' strain energy

1. Introduction

Basically, three criteria of strength, stiffness, and elastic stability are considered in the design of structures. The criterion of strength originates in the precept that the stresses applied to a structure by the influence of external forces should not exceed the allowable amount. Also, the criterion of stiffness determines that the elastic displacements of a structure should not exceed the allowable limit. Last but not least, the criterion of elastic stability avoids buckling of the compression members. To determine the dimensions and geometric characteristics of the sections of structural members, Although the criterion of strength is decisive in most cases, stiffness is dominant every so often. To ensure the safety of braced frames against elastic drift during the linear design process, appropriate elastic stiffness needs to be provided by the bracing system. The necessity of meeting the elastic stiffness requirement of bracing systems is well established in the literature (Sabelli *et al*. 2003, Pan *et al*. 2018, Pan and Tong 2020 and Liu and Helwing 2020). Developing a practical, effective and reliable approach to evaluate the lateral stiffness of braced steel frames is a major challenge for engineers. However, few studies have been conducted to determine the elastic stiffness required for bracing systems (Grande and Rasulo 2013, Fateh *et al*. 2016 and MacRae *et al*. 2016).

Curved beams are more efficient than straight ones in transferring loads considering the fact that the load transfer is affected by bending, shear and membrane action. Some structures like arches and arch bridges are modeled by curved beam elements. A significant amount of research has been devoted to the development of curved beam elements in recent decades since making use of such elements in structures is a versatile method of solving structural and other mechanical problems (Love 1944, Michalos 1958, Holmes 1957, Palaninathan and Chandrasekharan 1985, Marquis and Wang 1989, Haktanir 1995, Yu 2004, Yu and Nie 2005 and 2007, Yu *et al*. 2006, and Yu 2006). A majority of the numerical studies have mainly focused on the exact strain energy or natural shape function while others are based on assumed displacement fields (Kardestuncer 1974, Morris 1968, Petrolo and Casciaro 2004, Moradipour 2015 and Wang *et al*. 2013).

Dawe (1974) evaluated the performance of curved-beam finite element models of the circular center line with different types of strain displacement equations so as to

*Corresponding author, Ph.D. Research Assistant
E-mail: Habib.GhasemiJouneghani@uts.edu.au
[a]Associate Professor
E-mail: fanaie@kntu.ac.ir
[b]Ph.D.
E-mail: talebika@ualberta.ca
[c]Lecturer
E-mail: Mina.Mortazavi@uts.edu.au

ISSN: 1229-9367 (Print), 1598-6233 (Online)

come up with solutions to circular arch problems. His models showed oscillatory behavior in calculating the force in thin arches. Dawe (1974) extended his previous work to include circular arches through the corresponding exact strain element equations. The same conclusions were drawn in this research project.

Yamada and Ezawa (1977) presented an exact stiffness matrix for the circular curved element. They assumed that the shape functions considered in the finite element models provided the exact deformations of circular arches and proved that they were the inverse of the flexibility matrix in a comparison between the inverse of the derived stiffness matrix and the exact one. Just (1982) presented an exact stiffness matrix for a circular curved beam subjected to in-plane loading. The matrix was derived from the governing differential equations through the finite element procedure.

Litewaka and Rakowski (1988) derived the exact stiffness matrix for a curved beam element with constant curvature. Two plane nodes with six degrees of freedom were considered by taking the effect of flexural, axial and shear deformations into account. The analytical shape functions describing radial and tangential displacements, as well as cross sectional rotations in algebraic trigonometric form, were presented by incorporating the coupled shear and membrane effects. Based on the shape functions, using the strain energy formula, the stiffness matrix for the flexible and compressible shear arch element was formulated. Gimena *et al*. (2008) obtained the equivalent load vector and the stiffness matrix of a 3D-curved beam element with a variable cross-section under generalized loads through a linear ordinary differential equation governing its structural behavior. Gimena *et al*. (2008) studied the simulation of the structural behavior of a general curved beam element in a Cartesian coordinate system under generalized loads such as the circular arch and balcony. They provided the exact analytical solutions and expressions of transfer and stiffness matrices for widely spread cases of curved beams.

Rezaiee and Rajabzadeh (2016) presented an explicit stiffness matrix by a closed-form solution through the stiffness-based finite element method for a parabolic beam element with two nodes and six degrees of freedom. They concluded that applying the suggested explicit form of the curved beam stiffness matrix could remarkably accelerate the analysis procedure. Muhaisin (2003) presented a new form of the stiffness matrix for a reinforced concrete plane frame element including the effect of shear deformations. The layered approach was adopted to consider the effect of variations in material properties on thickness. He achieved satisfying results compared to other studies. Hadi (2002) derived a curved beam stiffness matrix by taking the effect of shear, axial and bending deformations into account. For this purpose, a curved beam element with hinges at one or both ends was developed and a good accordance was obtained with other studies.

Li *et al*. (2012) assessed the exact solutions for in-plane displacements of curved beams with pinned-pinned ends based on the theory of virtual work and the principle of thermal elasticity. Upadhyay et.al. (2018) derived a stiffness matrix for the unknown displacements and rotations of a

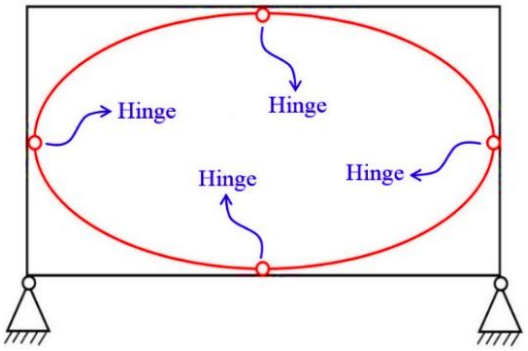

Fig. 1 Side view of the steel moment frame equipped with elliptic brace

curved beam subjected to horizontal and vertical loads and moments at the ends by using the strain energy concept, Castigliano's theorem and the basic mechanics. The obtained final element stiffness matrix was applicable to a variety of curved beam samples with practical use, e.g., arches, hooks and curved traffic poles subjected to various loading conditions. Horibe and Mori (2015) reviewed in-plane and out-of-plane deflections of a J-shaped beam, which was clamped at one end and was free at the other, subjected to a point load (both in-plane and out-of-plane loads). An analytical solution based on Castigliano's theorem was adopted through numerical integration of the modified elliptic integral and differentiation of the beam's strain energy. They found that when out-of-plane and in-plane loads acted simultaneously on a J-shaped beam, the stresses or deflections of the beam could be estimated according to each result. Dahlberg (2004) evaluated the deflections of curved beams in two ways through a well-known energy method (the Castigliano theorem). In the first example, the curved beam in the form of a quarter of an ellipse was clamped at one end and was free at the other. A force P was applied to the free end perpendicular to the plane of the curved beam. In the second example, a half-elliptic beam was clamped at both ends subjected to a force *P* at the center of the beam.

Xie *et al*. (2020) evaluated the hysteretic model and experimental validation of a Full-scale variable damping self-centering brace through cyclic tests. They have shown that this brace presents a quasi-flag-shaped behavior, which provides reliable energy dissipation. Xu *et al*. (2021) presented an innovative self-centering steel buckling-restrained brace (SC-SBRB) consisting of two independent and complementary systems, i.e., a buckling-restrained energy-dissipation system and a pre-compressed disc spring self-centering system. They investigated the working mechanism and mechanics of the SC-SBRB under one cycle of cyclic loading. A good agreement between the simulation results and the prediction results confirms the validity of the proposed self-centering hysteretic model. Xu *et al*. (2022) investigated a pre-pressed spring self-centering energy dissipation (PS-SCED) bracing system. They proposed and verified a novel force method-based hysteretic analysis model that governs the distribution of the internal force by a numerical model of the PS-SCED brace

and tests of the PS-SCED brace specimen. They showed that the proposed brace has significant energy dissipation and re-centering abilities.

This study deals with a new elastoplastic lateral bracing system consisting of an elliptic central core in the middle of the frame named elliptic brace, as indicated in Fig. 1. The Elliptic-Braced Moment Resisting Frame (EBMRF) is a new lateral load system that when installed in the middle bay of the surrounding frames, not only prepares enough space for opening in the facade of a building but also provides an appropriate elastic stiffness and efficiency in the design and architecture. Moreover, this system can add to the aesthetics of a structure. In previous studies, the authors evaluated the seismic performance and failure mechanism of steel moment frames with elliptic bracing (Ghasemi *et al*. 2016, 2019, 2020, 2021 and 2022).

Ghasemi *et al*. (2022) presented a theoretical formula to calculate the elastic lateral stiffness in a two-dimensional single-story single-span simple steel frame equipped with elliptic brace. They have shown the error percentage between the elastic stiffness derived from the developed equations and that of the numerical analyses of finite element models was very low and negligible.

Achieving economical solutions to ensure the stability of bracing systems can be at least as important as benefitting from the advantage of the equation between stiffness and strength. On the other hand, providing lateral stiffness in order to reduce elastic drifts is of primary concerns in the design process of braced steel structures. This should be done in such a way that the placement of the brace element in the structure by the design engineer does not disrupt its architecture. It appears that introducing a precise formulation to determine the amounts of elastic stiffness and elastic drift amplification or the percentage of stiffness variation when using the elliptic brace in a common story of steel moment frame can pave the way for a more accurate design and the control of elliptic-braced moment frames. On the other hand, it leads to a more in-depth understanding of the elastic behavior of the elliptic brace in ELBSF. This study aims to provide an exact formulation to determine the amount of elastic stiffness in a typical story of EBMRF. In this regard, a simple, linear and accurate formula is presented to estimate the elastic drift and elastic stiffness according to the type of the profile of the elliptic brace utilized in the story. To this end, first, an exact approach alongside the energy method (Hibbeler, 2018) is presented to calculate elastic drift of a single-story single-span EBMRF, which can be solved by the existing mathematical software. All effective factors are taken into account, including axial and shear loads as well as bending moment in the elliptic brace. At the end of the analysis, the lateral stiffness of the EBMRF system can be calculated by an improved and innovative relation through the energy method based on the geometric properties of the employed sections and specifications of the used material. The proposed method is presented in Section 2 by the applied concepts of strain energy and Castigliano's theorem in the structural analysis. A distinct linear formula covering all steel profiles of the elliptic brace is proposed to calculate the amount of elastic stiffness or the percentage of stiffness variations in an EBMRF. This formula can be readily implemented by engineers, either in manual or in a software design process.

In the current study, first, a practical and effective equation to determine the elastic lateral stiffness through an improved and innovative formulation for a two-dimensional single-story single-span EBMRF under lateral load is presented. Then the proposed relation is evaluated through various examples. The results indicate that the error percentage between the elastic stiffness values derived by the developed equations and the numerical results from the finite element model is very small and negligible. Alternative structural elements of the elliptic brace are presented in a one-story base model to demonstrate the advantages of the proposed system. The equivalent element for the elliptic brace can contribute to its accurate and easy modeling and design. The results reveal that the percentage of error between the elastic stiffness values obtained by the developed equations and those of the finite element numerical analysis is insignificant.

2. A new procedure for calculating elastic stiffness of a two-dimensional single-story single-span elliptic-braced steel frame with rigid connections

In this section, first, the exact amount of elastic lateral stiffness is calculated using the analytical method of strain energy (Hibbeler 2018) for a two-dimensional single-story single-span steel moment frame with directly welded beam-to-column rigid connections equipped with an elliptic brace (EBMRF) subjected to the lateral force P (Fig. 2(a)). Hinges are used to connect the four quarters of elliptic braces to each other. As illustrated in Fig. 2(b), the desired elliptic-braced steel moment frame can be turned into a half-frame using the technique of structural analysis modeling relating to symmetric structures with anti-symmetric loading. Considering the directly welded beam-to-column rigid connections of the elliptic-braced steel half-frame and simple connections of the elliptic brace to the steel half-frame, as depicted in Fig. 2(b), the geometric characteristics are expressed in Eq. (1):

$$\begin{aligned} &a = \frac{L_b}{2} \quad , \quad b = \frac{L_c}{2} \\ &tan\theta = \frac{b}{a} = \frac{L_c}{L_b} = e \\ &sin\theta = \frac{b}{\sqrt{a^2 + b^2}} = \frac{e}{\sqrt{1 + e^2}} \\ &cos\theta = \frac{a}{\sqrt{a^2 + b^2}} = \frac{1}{\sqrt{1 + e^2}} \end{aligned} \tag{1}$$

Meanwhile, θ was introduced as a parameter. According to Fig. 2(b), using the compatibility equation for elliptic-braced steel half-frame, the vertical component of reaction at support B is calculated as follows:

$$\begin{aligned} \sum F_y = 0 \quad &\rightarrow \quad R_B + R_C = \frac{PL_c}{L_b} \\ &\rightarrow \quad R_B = \frac{PL_c}{L_b} - R_C \end{aligned} \tag{2}$$

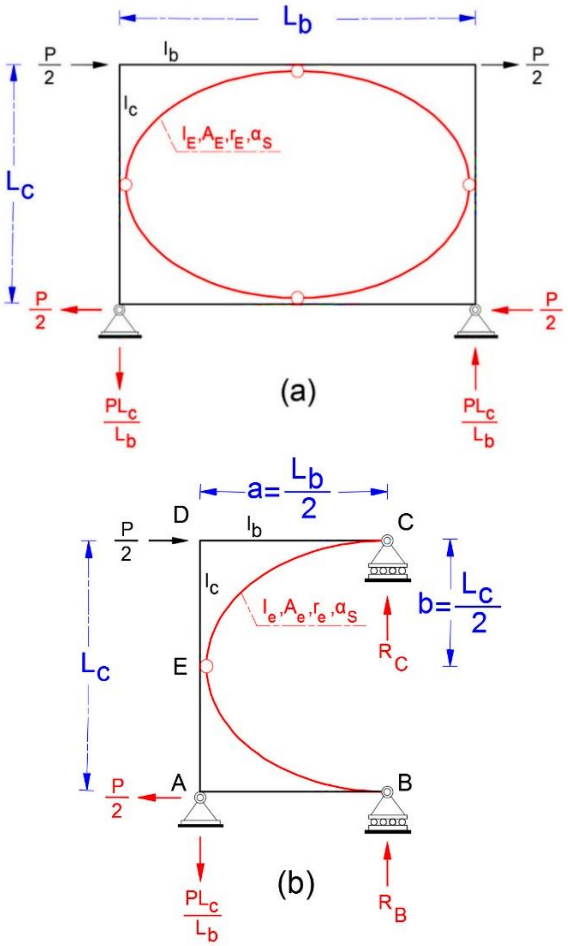

Fig. 2 The analysis of the EBMRF after changing into two half-frames; (a) the desired steel moment frame with directly welded rigid connections equipped with the elliptic brace and (b) the half-braced frame after splitting the steel moment frame

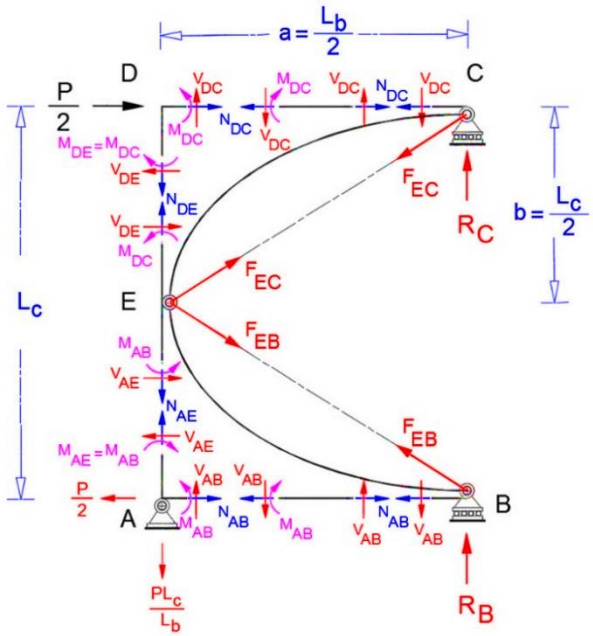

Fig. 3 The internal actions of the elliptic-braced steel half-frame elements

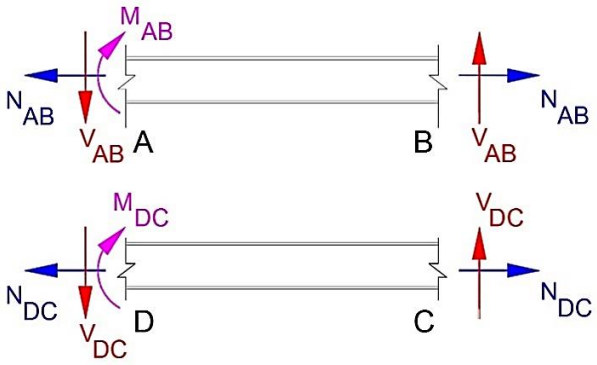

Fig. 4 The internal actions of beams DC and AB

Where P denotes the lateral shear force applied to the elliptic-braced steel moment frame, and L_b and L_c are used for the beam and column length (distance between centerlines), respectively. The internal actions diagram for the elliptic-braced steel half-frame elements is shown in Fig. 3. As indicated in Fig. 4, by adopting the static equations for the elliptic-braced steel half-frame, the internal force of the beams AB and CD is calculated by Eqs. (2) and (3), respectively. The values of the shear force and axial force at both ends of DC and AB members are equal. In other words, $V_{ij} = V_{ji}$ and $N_{ij} = N_{ji}$.

$$\sum M_C = 0 \quad \rightarrow \quad M_{DC} = V_{DC}\frac{L_b}{2} \quad \rightarrow \quad V_{DC} = \frac{2M_{DC}}{L_b} \tag{3}$$

$$\sum M_B = 0 \quad \rightarrow \quad M_{AB} = V_{AB}\frac{L_b}{2} \quad \rightarrow \quad V_{AB} = \frac{2M_{AB}}{L_b} \tag{4}$$

Using the compatibility equations in nodes A, B, C and D, the internal force in the members of the elliptic-braced steel half-frame is calculated as follows (Figs. 5(a) to 5(d)).

$$\sum F_y = 0 \quad \rightarrow \quad R_C - F_{EC}sin\theta - V_{CD} = 0 \quad \rightarrow \quad F_{EC} = \frac{R_C}{sin\theta} - \frac{V_{DC}}{sin\theta} \tag{5}$$

$$\sum F_x = 0 \quad \rightarrow \quad N_{DC} = -F_{EC}cos\theta \tag{6}$$

Incorporating Eq. (3) into Eq. (5) leads to the constituent terms of Eq. (5) as follows:

$$F_{EC} = \frac{R_C}{sin\theta} - \frac{2M_{DC}}{L_b sin\theta} \tag{7}$$

Incorporating Eq. (7) into Eq. (6) and using geometrical Eq. (1) lead to the constituent terms of Eq. (6) as follows:

$$N_{DC} = \frac{2M_{DC}}{L_b tan\theta} - \frac{R_C}{tan\theta} = \left(\frac{2M_{DC}}{L_b e} - \frac{R_C}{e}\right) \tag{8}$$

For node B:

$$\sum F_y = 0 \quad \rightarrow \quad F_{EB} = -\frac{R_B}{sin\theta} + \frac{V_{AB}}{sin\theta} \tag{9}$$

$$\sum F_x = 0 \quad \rightarrow \quad N_{AB} = -F_{EB}cos\theta \tag{10}$$

Incorporating Eqs. (2) and (4) into Eq. (9) results in the constituent terms of Eq. (9) as follows:

$$F_{EB} = -\frac{\frac{PL_c}{L_b} + R_C}{sin\theta} + \frac{2M_{AB}}{L_b sin\theta} \tag{11}$$

Incorporating Eq. (11) into Eq. (10) and using geometrical Eq. (1) give the constituent terms of Eq. (10) as follows:

$$N_{AB} = \frac{\frac{PL_c}{L_b} - R_C}{tan\theta} - \frac{2M_{AB}}{L_b tan\theta} = \left(P - \frac{R_C}{e} - \frac{2M_{AB}}{L_b e}\right) \tag{12}$$

For node *A*:

$$\sum F_y = 0 \quad \rightarrow \quad N_{AE} + V_{AB} = \frac{PL_c}{L_b} \tag{13}$$

$$\sum F_x = 0 \quad \rightarrow \quad V_{AE} = N_{AB} - \frac{P}{2} \tag{14}$$

Using geometric Eq. (1) and incorporating Eq. (4) into Eq. (13) and Eq. (12) into Eq. (14) lead to the terms of Eqs. (13) and (14), respectively as follows:

$$N_{AE} = \frac{PL_c}{L_b} - \frac{2M_{AB}}{L_b} = e\left(P - \frac{2M_{AB}}{L_c}\right) \tag{15}$$

$$V_{AE} = \frac{\frac{PL_c}{L_b} - R_C}{tan\theta} - \frac{2M_{AB}}{L_b tan\theta} - \frac{P}{2} = \frac{P}{2} - \frac{R_C}{e} - \frac{2M_{AB}}{L_b e} \tag{16}$$

For node *D*:

$$\sum F_y = 0 \quad \rightarrow \quad N_{DE} = V_{DC} = \frac{2M_{DC}}{L_b} = \frac{2M_{DC}}{L_c} e \tag{17}$$

$$\sum F_x = 0 \quad \rightarrow \quad V_{DE} = \frac{P}{2} + N_{DC} \tag{18}$$

Incorporating Eq. (11) into Eq. (10) gives the terms of Eq. (10) as follows:

$$V_{DE} = \frac{P}{2} + \frac{2M_{DC}}{L_b tan\theta} - \frac{R_C}{tan\theta} = \frac{P}{2} + \frac{2M_{DC}}{L_b e} - \frac{R_C}{e} \tag{19}$$

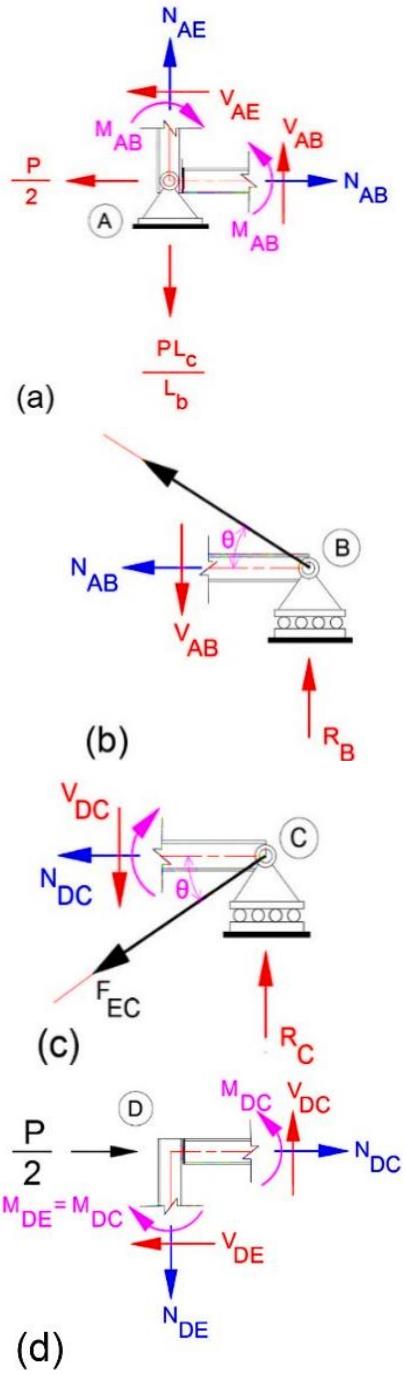

Fig. 5 Analysis of joints in the elliptic-braced steel half-frame; a) joint *A*, b) joint *B*, c) joint *C*, and d) joint *D*

2.1 Strain energy of the elliptic brace

To calculate the strain energy in the elliptic brace quarter elements *EC* and *EB*, all the effects of axial, shear and bending deformation are taken into account. The governing equation for the ellipse is calculated by Eq. (A-14), as shown in Fig.6 (a). The infinitesimal arc length (ds) on the ellipse for any desired point in coordinates *(x, y)* is calculated by Eq. (20):

$$\frac{x^2}{a^2} + \frac{y^2}{b^2} = 1 \quad \rightarrow \quad y = b\sqrt{1 - \frac{x^2}{a^2}} \quad , \quad 0 \le x \le a \tag{20}$$

$$ds = \sqrt{dx^2 + dy^2} = \sqrt{1 + y'^2}dx \tag{21}$$

From the elliptic equation (Eq. 20), the inclination angle of the tangent line from any point relative to the horizontal axis (ϕ) on the elliptic brace is calculated by Eq. (22):

$$-y' = b\frac{\frac{x}{a^2}}{\sqrt{1 - \frac{x^2}{a^2}}} = tan\,\phi \tag{22}$$

As shown in Fig. 6(a), by considering the ellipse in the

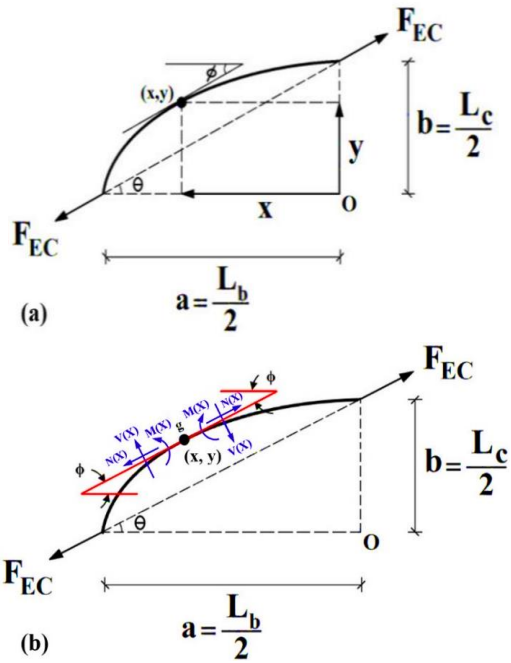

Fig. 6 Analysis of the quarter elliptic-brace (a) configuration of the quarter elliptic-brace (b) the internal actions of the element *EC* in the quarter elliptic-brace

second quarter of the coordinate system, the negative sign in Eq. (22) to calculate the acute angle is ignored. Making use of trigonometric relations in Eq. (22) leads to the terms of Eq. (22) as follows:

$$1+tan^2\phi=\frac{1}{cos^2\phi}\quad\rightarrow\quad cos^2\phi=\frac{1}{1+tan^2\phi}$$
$$=\frac{1}{1+\frac{b^2\frac{x^2}{a^4}}{1-\frac{x^2}{a^2}}}=\frac{1}{\frac{1-\frac{x^2}{a^2}+\frac{b^2x^2}{a^4}}{1-\frac{x^2}{a^2}}}=\frac{1-\frac{x^2}{a^2}}{1-\frac{x^2}{a^2}+\frac{b^2x^2}{a^4}} \tag{23}$$
$$\rightarrow\quad cos\phi=\sqrt{\frac{1-\frac{x^2}{a^2}}{1-\frac{x^2}{a^2}+\frac{b^2x^2}{a^4}}}$$

$$sin^2\phi=1-cos^2\phi=\frac{1-\frac{x^2}{a^2}+\frac{b^2x^2}{a^4}-1+\frac{x^2}{a^2}}{1-\frac{x^2}{a^2}+\frac{b^2x^2}{a^4}}$$
$$=\frac{\frac{b^2x^2}{a^4}}{1-\frac{x^2}{a^2}+\frac{b^2x^2}{a^4}}\rightarrow\quad sin\phi=\frac{b\frac{x}{a^2}}{\sqrt{1-\frac{x^2}{a^2}+\frac{b^2x^2}{a^4}}} \tag{24}$$

The $sin\phi$ and $cos\phi$ are functions of the parameter x. Using the equations of static equilibrium, according to Fig. 6(b), the internal actions (axial, shear forces, and bending moment) of the elliptic brace are obtained by Eqs. (25) to (27) as follows:

$$\sum F_x=0\quad\rightarrow\quad Fcos\theta=N(x)cos\phi+V(x)sin\phi \tag{25}$$

$$\sum F_y=0\quad\rightarrow\quad Fsin\theta=N(x)sin\phi-V(x)cos\phi \tag{26}$$

$$\sum M_g=0\quad\rightarrow\quad M(x)=-Fb\left(1-\sqrt{1-\frac{x^2}{a^2}}\right)cos\theta+F(x)sin\theta \tag{27}$$

The angle of θ is constant for an specific frame. solving the system of Eqs. (25) and (26), the values of axial force and shear force for the quarter of elliptic element are calculated in terms of x by Eqs. (28) and (29), respectively as follows:

$$N(x)=F(cos\theta cos\phi+sin\theta sin\phi) \tag{28}$$

$$V(x)=F(cos\theta sin\phi-sin\theta cos\phi) \tag{29}$$

By summing Eq. (27), Eq. (28) and Eq. (29), the total amount of strain energy for each element of the quarter elliptic brace is calculated as follows:

$$\begin{aligned}U_{elliptic\ \ brace,bav}&=U_b+U_a+U_v\\&=\int_0^a\frac{M(x)^2}{2EI_e}\sqrt{1+y'^2}dx\\&+\int_0^a\frac{N(x)^2}{2EA_e}\sqrt{1+y'^2}dx\\&+\int_0^a\frac{V(x)^2}{2GA_e}\sqrt{1+y'^2}dx\end{aligned} \tag{30}$$

Where

$$\sqrt{1+y'^2}=\sqrt{1+\frac{b^2\frac{x^2}{a^4}}{1-\frac{x^2}{a^2}}}=\sqrt{\frac{1-\frac{x^2}{a^2}+b^2\frac{x^2}{a^4}}{1-\frac{x^2}{a^2}}} \tag{31}$$

Where $G=\frac{E}{2(1+\upsilon)}$ presents the modulus of rigidity, $\upsilon=0.3$is the Poisson's ratio, A_e indicates the cross-sectional area of the elliptic brace, E (200,000 MPa) is used for the elastic modulus of the used steel, I_e presents the moment of inertia of the elliptic brace about the bending axis (strong axis), and α_s is used for the shape dependent factor for shear, which is equal to 1.2 for a rectangular section, 2 for a HSS section, and $\frac{10}{9}$ for a pipe section. Moreover, it is equal to the ratio of the area of the entire section to the area of the web (A/ht) for I-sections, box sections, and channels (h is the elliptic depth and t is the web thickness).

By placing Eqs. (1), (26), and (30) in U_b presented in Eq. (29), the strain energy due to the bending moment in the quarter elliptic brace is calculated as follows:

$$\begin{aligned}U_b&=\frac{F^2}{2EI_e}\int_0^a\left[-bcos\theta\left(1-\sqrt{1-\frac{x^2}{a^2}}\right)+sin\theta.x\right]^2\\&\times\frac{\sqrt{1-\frac{x^2}{a^2}+b^2\frac{x^2}{a^4}}}{\sqrt{1-\frac{x^2}{a^2}}}dx\\&=\frac{F^2b^2}{2EI_e(1+e^2)}\int_0^a\left[-\left(1-\sqrt{1-\frac{x^2}{a^2}}\right)+\frac{x}{a}\right]^2\\&\times\frac{\sqrt{1-\frac{x^2}{a^2}+e^2\frac{x^2}{a^2}}}{\sqrt{1-\frac{x^2}{a^2}}}dx\end{aligned} \tag{32}$$

To calculate the integral of Eq. (32), the change of variable is implemented according to Eq. (33).

$$t = \frac{x}{a} \qquad \rightarrow \qquad dx = adt \tag{33}$$

Incorporating Eq. (33) into Eq. (32) leads to the terms of Eq. (32) as follows:

$$U_b = \frac{F^2 b^2 a}{2EI_e}\int_0^1 \frac{\left[-1+t+\sqrt{1-t^2}\right]^2\sqrt{1+(e^2-1)t^2}}{(1+e^2)\sqrt{1-t^2}}dt \tag{34}$$

If,

$$\Psi_b(e) = \int_0^1 \frac{\left[-1+t+\sqrt{1-t^2}\right]^2\sqrt{1+(e^2-1)t^2}}{(1+e^2)\sqrt{1-t^2}}dt \tag{35}$$

$\Psi_b(e)$ is presented as per aspect ratio (e) and can be calculated numerically. $\Psi_b(e)$ is graphically shown in Fig 7 for different values of e. By incorporating Eq. (35) into Eq. (34), the strain energy due to the bending moment in the quarter elliptic brace is calculated as follows:

$$U_b = \frac{F^2 b^2 a}{2EI_e}\Psi_b(e) \tag{36}$$

By placing Eqs. (1), (23), (24), (28), and (31) in U_v presented in Eq. (30), the strain energy due to the axial force in the quarter elliptic brace is calculated as follows:

$$\begin{aligned} U_a &= \frac{F^2}{2EA_e}\int_0^a [cos\theta cos\phi + sin\theta sin\phi]^2 \times \frac{\sqrt{1-\frac{x^2}{a^2}+e^2\frac{x^2}{a^2}}}{\sqrt{1-\frac{x^2}{a^2}}}dx \\ &= \frac{F^2}{2EA_e}\int_0^a \left[\frac{1}{\sqrt{1+e^2}}\frac{\sqrt{1-\frac{x^2}{a^2}}}{\sqrt{1-\frac{x^2}{a^2}+e^2\frac{x^2}{a^2}}} + \frac{e}{\sqrt{1+e^2}}\frac{e\frac{x}{a}}{\sqrt{1-\frac{x^2}{a^2}+e^2\frac{x^2}{a^2}}}\right]^2 \times \frac{\sqrt{1-\frac{x^2}{a^2}+e^2\frac{x^2}{a^2}}}{\sqrt{1-\frac{x^2}{a^2}}}dx \end{aligned} \tag{37}$$

To calculate the integral of Eq. (37), the change of variable is used according to Eq. (33). Incorporating Eq. (33) into Eq. (37) leads to the terms of Eq. (37) as follows:

$$U_a = \frac{F^2 a}{2EA_e}\int_0^1 \frac{1}{(1+e^2)}\frac{\left[\sqrt{1-t^2}+e^2 t\right]^2}{\sqrt{(1-t^2)[1+(e^2-1)t^2]}}dt \tag{38}$$

If

$$\Psi_a(e) = \int_0^1 \frac{1}{(1+e^2)}\frac{\left[\sqrt{1-t^2}+e^2 t\right]^2}{\sqrt{(1-t^2)[1+(e^2-1)t^2]}}dt \tag{39}$$

$\Psi_a(e)$ is merely a function of the parameter e and can be numerically solved. The value of $\Psi_a(e)$ for different values of e is shown graphically in Fig. 7. By incorporating Eq. (39) into Eq. (38), the strain energy due to the axial force in the quarter elliptic brace is calculated as follows:

$$U_a = \frac{F^2 a}{2EA_e}\Psi_a(e) \tag{40}$$

By placing Eqs. (1), (23), (24), (29), and (31) in U_v presented in Eq. (30), the strain energy due to the shear force in the quarter elliptic brace is calculated as follows:

$$\begin{aligned} U_v &= \frac{\alpha_s . F^2}{2GA_e}\int_0^a [cos\theta sin\phi - sin\theta cos\phi]^2 \times \frac{\sqrt{1-\frac{x^2}{a^2}+e^2\frac{x^2}{a^2}}}{\sqrt{1-\frac{x^2}{a^2}}}dx \\ &\rightarrow U_v = \alpha_s\frac{F^2}{2GA_e}\int_0^a \left[\frac{1}{\sqrt{1+e^2}}\frac{e\frac{x}{a}}{\sqrt{1-\frac{x^2}{a^2}+e^2\frac{x^2}{a^2}}} - \frac{e}{\sqrt{1+e^2}}\frac{\sqrt{1-\frac{x^2}{a^2}}}{\sqrt{1-\frac{x^2}{a^2}+e^2\frac{x^2}{a^2}}}\right]^2 \times \frac{\sqrt{1-\frac{x^2}{a^2}+e^2\frac{x^2}{a^2}}}{\sqrt{1-\frac{x^2}{a^2}}}dx \end{aligned} \tag{41}$$

To calculate the integral of Eq. (41), the change of variable is employed according to Eq. (33). Incorporating Eq. (33) into Eq. (41) leads to the constituent terms of Eq. (41) as follows:

$$U_v = \alpha_s\frac{F^2 a}{2GA_e}\int_0^1 \frac{e^2}{(1+e^2)}\frac{\left[t-\sqrt{1-t^2}\right]^2}{\sqrt{(1-t^2)[1+(e^2-1)t^2]}} \tag{42}$$

If

$$\Psi_v(e) = \int_0^1 \frac{e^2}{(1+e^2)}\frac{\left[t-\sqrt{1-t^2}\right]^2}{\sqrt{(1-t^2)[1+(e^2-1)t^2]}}dt \tag{43}$$

$\Psi_v(e)$ is only a function of the parameter e and can be numerically solved. The value of $\Psi_v(e)$ for different values of e is shown graphically in Fig. 8. By incorporating Eq. (43) into Eq. (42), the strain energy due to the shear force in the quarter elliptic brace is calculated by Eq. (44) as follows:

$$U_v = \alpha_s\frac{F^2 a}{2GA_e}\Psi_v(e) \tag{44}$$

The parameters $\Psi_b(e), \Psi_a(e)$ and $\Psi_v(e)$ are merely functions of the parameter e and can be numerically solved. The values of $\Psi_b(e), \Psi_a(e)$ and $\Psi_v(e)$ for different values of e are shown graphically in Fig. 7.

Incorporating Eqs. (36), (40) and (44) into Eq. (30) leads to the strain energy saved in each quarter elliptic brace as follows:

$$U_{elliptic\ \ brace,bav} = \frac{F^2.a}{2EA_e}\frac{\Psi_{bav}}{1+e^2} \tag{45}$$

By placing Eqs. (1), (7) and (11) in Eq. (45), the strain energy saved in each quarter elliptic brace (*EC* and *EB*) can be calculated as follows:

$$U_{EC} = \frac{L_b}{4EA_e}\left[\frac{R_C\sqrt{1+e^2}}{e} - 2M_{DC}\frac{\sqrt{1+e^2}}{L_c}\right]^2\frac{\Psi_{bav}}{1+e^2} \tag{46}$$

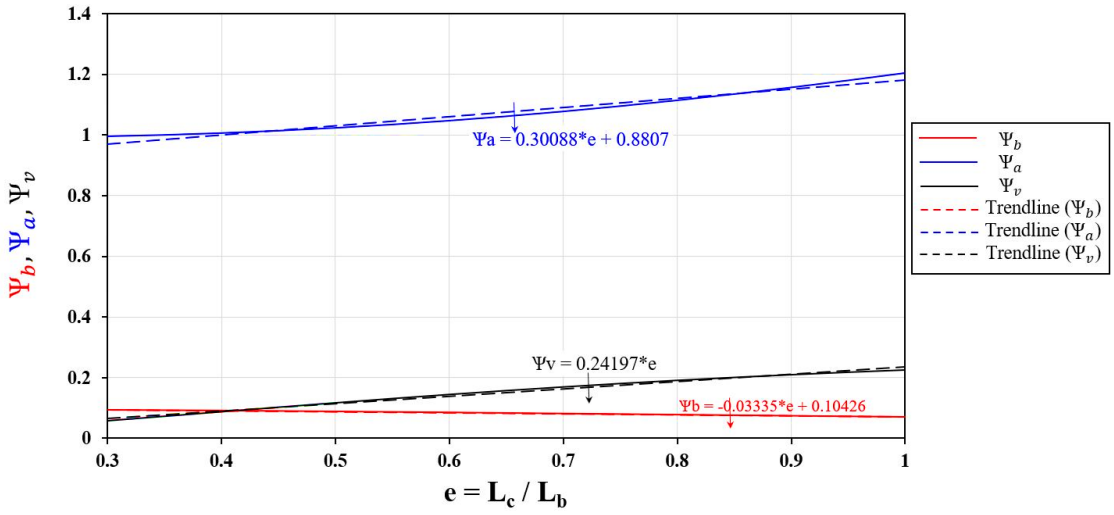

Fig. 7 $\Psi_b(e)$,$\Psi_a(e)$, and $\Psi_v(e)$ as a function of parameter e

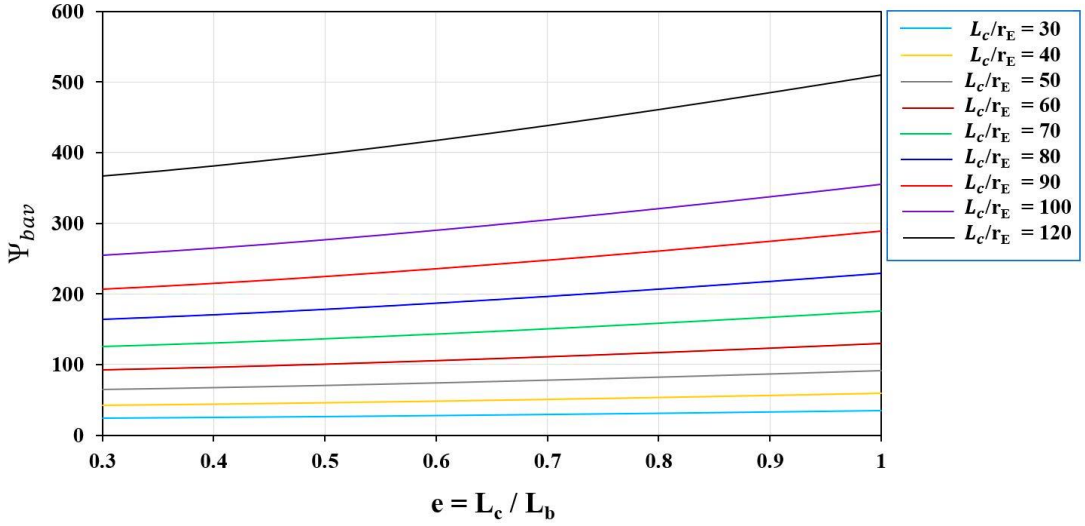

Fig. 8 $\Psi_{bav}(e)$ as a function of parameter e

$$U_{EB} = \frac{L_b}{4EA_e}\left[-P\sqrt{1+e^2} + \frac{R_C\sqrt{1+e^2}}{e} + 2M_{AB}\frac{\sqrt{1+e^2}}{L_c}\right]^2 \frac{\Psi_{bav}}{1+e^2} \quad (47)$$

Where the parameter Ψ_{bav} is defined by Eq. (48) as below:

$$\Psi_{bav} = \left[\left(\frac{L_c}{r_e}\right)^2 \frac{\Psi_b}{4} + 2.6\alpha_s\Psi_v + \Psi_a\right](1+e^2) \quad (48)$$

It can be seen that the parameter $\Psi_{bav}(e)$ is only a function of the parameter e. Therefore, it can be numerically solved.

The value of $\Psi_{bav}(e)$ for different values of e is shown graphically in Fig. 8.

By placing the linearly fitted values for the diagrams $\Psi_b(e)$,$\Psi_a(e)$ and $\Psi_v(e)$ from Fig. 7 in Eq. (48), $\Psi_{bav}(e)$ can be calculated approximately by the following relation.

$$\Psi_{bav} = \left[\left(\frac{L_c}{r_e}\right)^2 (-0.0083375e+0.026065) + 2.6\alpha_s(0.24197e - 0.0069) + (0.30088e + 0.8807)\right](1+e^2) \quad (49)$$

By summing Eq. (46) and Eq. (47), the total value of strain energy in half of the elliptic brace is calculated as follows:

$$U_{elliptic\ \ brace,bav} = \frac{L_b\Psi_{bav}}{4EA_e}\left[\left(\frac{R_C}{e} - \frac{2M_{DC}}{L_c}\right)^2 + \left(-P + \frac{R_C}{e} + \frac{2M_{AB}}{L_c}\right)^2\right] \quad (50)$$

2.2 Strain energy of the elliptic braced frame

By summing the values of strain energy due to the bending deformation for the column elements (elements *AE*

and *DE*) as well as the bending deformation for the beam elements (elements *AB* and *DC*) as well as calculating the total values of strain energy in half of the elliptic brace due to axial and shear forces and bending moment (elements *EC* and *EB*), the total amount of strain energy for the elliptic-braced steel half-frame is calculated as follows

$$\begin{aligned} U &= U_{column} + U_{beams} + U_{elliptic\ \ brace,bav} \\ U &= \frac{L_c}{48EI_c}\left[\left(1+\frac{12\alpha_{s,c}r_c^2}{L_c^2}\right)\left(\frac{PL_c}{2}-R_CL_b-2M_{AB}\right)^2+\left(1+\frac{12\alpha_{s,c}r_c^2}{L_c^2}\right)\left(\frac{P}{2}L_c-R_CL_b+2M_{DC}\right)^2\right. \\ &\quad \left.+3PL_c(M_{AB}-M_{DC})+6R_CL_b(M_{DC}-M_{AB})\ \ +\frac{12e^2r_c^2}{L_c^2}(4M_{DC}^2-(PL_c-2M_{AB})^2)\right] \\ &\quad +\frac{L_b}{12EI_b}\left[\left(1+\frac{12\alpha_{s,b}r_b^2}{L_b^2}\right)(M_{AB}^2+M_{DC}^2)+\frac{3r_b^2}{e^2L_b^2}((PL_c-R_CL_b-2M_{AB})^2+(2M_{DC}-R_CL_b)^2)\right] \\ &\quad +\frac{L_b\Psi_{bav}}{4EA_e}\left[\left(\frac{R_C}{e}-\frac{2M_{DC}}{L_c}\right)^2+\left(-P+\frac{R_C}{e}+\frac{2M_{AB}}{L_c}\right)^2\right] \end{aligned} \tag{51}$$

The parameters T, S, Q, λ_b, η_b, λ_c, η_c and β are defined for the initial simplification of the above equations as follows:

$$T=\frac{L_b\Psi_{bav}}{4EA_e} \tag{52}$$

$$S=\frac{L_c}{48EI_c},\quad \lambda_c=1+12\frac{\alpha_{s,c}}{\left(\frac{L_c}{r_c}\right)^2}\ ,\quad \eta_c=12\frac{e^2}{\left(\frac{L_c}{r_c}\right)^2} \tag{53}$$

$$Q=\frac{L_b}{12EI_b},\quad \lambda_b=1+12\frac{\alpha_{s,b}}{\left(\frac{L_b}{r_b}\right)^2}\ ,\quad \eta_b=\frac{3}{e^2\left(\frac{L_b}{r_b}\right)^2} \tag{54}$$

$$\beta=\frac{I_b}{I_c} \tag{55}$$

Where, λ_b and λ_c present correction coefficients to consider the effects of the shear deformations in the beam and the column elements.

Also, η_b and η_c present correction coefficients to consider the effects of the axial deformations in the beam and the column elements.

As a result, it can be concluded that $\lambda_b \pm \eta_b \approx \lambda_b$ and $\lambda_c \pm \eta_c \approx \lambda_c$.

The stiffness ratio of the beam to the elliptic brace is defined by γ as follows:

$$\gamma=\frac{\frac{EI_b}{L_b^3}}{\frac{EA_e}{L_b}}=\frac{I_b}{A_eL_b^2} \tag{56}$$

Incorporating Eqs. (52), (53) and (54) into Eq. (51) leads to the terms of Eq. (51) as follows:

$$\begin{aligned} U &= T\left[\left(\frac{R_C}{e}-\frac{2M_{DC}}{L_c}\right)^2+\left(-P+\frac{R_C}{e}+\frac{2M_{AB}}{L_c}\right)^2\right] \\ &\quad +S\left[\lambda_c\left(\frac{PL_c}{2}-R_CL_b-2M_{AB}\right)^2+\lambda_c\left(\frac{P}{2}L_c-R_CL_b+2M_{DC}\right)^2\right. \\ &\quad \left.+3PL_c(M_{AB}-M_{DC})+6R_CL_b(M_{DC}-M_{AB})\ \ +\eta_c(4M_{DC}^2-(PL_c-2M_{AB})^2)\right] \\ &\quad +Q[\lambda_b(M_{AB}^2+M_{DC}^2)+\eta_b((PL_c-R_CL_b-2M_{AB})^2+(2M_{DC}-R_CL_b)^2)] \end{aligned} \tag{57}$$

According to Castigliano's second theorem, the first partial derivative of the total internal strain energy in a structure relative to the force applied to any point is equal to the deflection at the point of application of the force in the direction of its line of action. According to Fig. 2(b) and based on Castigliano's second theorem, the conditions of compatibility at joints *C*, *A* and *D* are defined by Eq. (58) as follows:

$$\Delta_{C_V}=\frac{\partial U}{\partial R_C}=0 \tag{58}$$

$$\Delta\theta_A=\frac{\partial U}{\partial M_{AB}}=0 \tag{59}$$

$$\Delta\theta_D=\frac{\partial U}{\partial M_{DC}}=0 \tag{60}$$

Using Cactigliano's second theorem in nodes C, A and D and placing Eq. (57) in Eqs. (58), (59) and (60), the systems of equations are obtained through:

$$\begin{aligned} &T\left[\frac{2}{e}\left(-P+\frac{2R_C}{e}+\frac{2M_{AB}}{L_c}-\frac{2M_{DC}}{L_c}\right)\right] \\ &\qquad +S[-2L_b\lambda_c(PL_c-2R_CL_b+2M_{DC}-2M_{AB}) \\ &+6L_b(M_{DC}-M_{AB})] \\ &\qquad +Q[-2L_b\eta_b(PL_c-2R_CL_b+2M_{DC}-2M_{AB})]=0 \\ &\rightarrow\left(\frac{4T}{e^2}+4\lambda_cL_b^2S+4\eta_bL_b^2Q\right)R_C \\ &\qquad +\frac{1}{L_b}\left(\frac{4T}{e^2}+(4\lambda_c-6)L_b^2S\right. \\ &\qquad \left.+4\eta_bL_b^2Q\right)M_{AB} \\ &\quad -\frac{1}{L_b}\left(\frac{4T}{e^2}+(4\lambda_c-6)L_b^2S+4\eta_bL_b^2Q\right)M_{DC} \\ &\qquad =\left(\frac{4T}{e^2}+4\lambda_cL_b^2S+4\eta_bL_b^2Q\right)P\frac{e}{2} \end{aligned} \tag{61}$$

By solving the systems of Eq. (62) to Eq. (63), the

$$
\begin{aligned}
&T\left[\frac{4}{L_c}\left(-P+\frac{R_C}{e}+\frac{2M_{AB}}{L_c}\right)\right]+S\left[-4\lambda_c\left(\frac{P}{2}L_c-R_CL_b-2M_{AB}\right)+3PL_c\right.\\
&\left.-6R_CL_b+4\eta_c(PL_c-2M_{AB})\right]+Q[2\lambda_bM_{AB}-4\eta_b(PL_c-R_CL_b-2M_{AB})]=0\\
&\rightarrow\left(\frac{4T}{e^2}+(4\lambda_c-6)L_b^2S+4\eta_bL_b^2Q\right)R_C+\frac{1}{L_b}\left(\frac{8T}{e^2}+8(\lambda_c-\eta_c)L_b^2S+(2\lambda_b+8\eta_b)L_b^2Q\right)M_{AB}\\
&\qquad=\left(\frac{4T}{e^2}-(3-2\lambda_c+4\eta_c)L_b^2S+4\eta_bL_b^2Q\right)Pe
\end{aligned}
\tag{62}
$$

$$
\begin{aligned}
&T\left[\frac{-4}{L_c}\left(\frac{R_C}{e}-\frac{2M_{DC}}{L_c}\right)\right]+S\left[4\lambda_c\left(\frac{P}{2}L_c-R_CL_b+2M_{DC}\right)-3PL_c+6R_CL_b+8\eta_cM_{DC}\right]\\
&+Q[2\lambda_bM_{DC}+4\eta_b(2M_{DC}-R_CL_b)]=0\\
&\rightarrow-\left(\frac{4T}{e^2}+(4\lambda_c-6)L_b^2S+4\eta_bL_b^2Q\right)R_C+\frac{1}{L_b}\left(\frac{8T}{e^2}+8(\lambda_c+\eta_c)L_b^2S+(2\lambda_b+8\eta_b)L_b^2Q\right)M_{DC}\\
&\qquad=\left((3-2\lambda_c)L_b^2S\right)Pe
\end{aligned}
\tag{63}
$$

unknowns M_{AB} and M_{DC} are obtained as follows:

Incorporating Eqs. (64) and (65) into Eq. (61) leads to

$$
\frac{M_{AB}}{L_b}=-\frac{\frac{4T}{e^2}+(4\lambda_c-6)L_b^2S+4\eta_bL_b^2Q}{\frac{8T}{e^2}+8(\lambda_c-\eta_c)L_b^2S+(2\lambda_b+8\eta_b)L_b^2Q}R_C+\frac{\frac{4T}{e^2}-(3-2\lambda_c+4\eta_c)L_b^2S+4\eta_bL_b^2Q}{\frac{8T}{e^2}+8(\lambda_c-\eta_c)L_b^2S+(2\lambda_b+8\eta_b)L_b^2Q}Pe \tag{64}
$$

$$
\frac{M_{DC}}{L_b}=\frac{\frac{4T}{e^2}+(4\lambda_c-6)L_b^2S+4\eta_bL_b^2Q}{\frac{8T}{e^2}+8(\lambda_c+\eta_c)L_b^2S+(2\lambda_b+8\eta_b)L_b^2Q}R_C+\frac{(3-2\lambda_c)L_b^2S}{\frac{8T}{e^2}+8(\lambda_c+\eta_c)L_b^2S+(2\lambda_b+8\eta_b)L_b^2Q}Pe \tag{65}
$$

the constituent terms of Eq. (61) as follows:

$$
R_C=a_1P \tag{66}
$$

Where

As a result, by assuming$\lambda_c+\eta_c\approx\lambda_c$and $\lambda_c-\eta_c\approx\lambda_c$:

$$
a_1=\frac{\left[\left(\frac{4T}{e^2}+4\lambda_cL_b^2S+4\eta_bL_b^2Q\right)-\frac{\left(\frac{4T}{e^2}+(4\lambda_c-6)L_b^2S+4\eta_bL_b^2Q\right)\left(\frac{4T}{e^2}-(3-2\lambda_c+4\eta_c)L_b^2S+4\eta_bL_b^2Q\right)}{\frac{4T}{e^2}+4(\lambda_c-\eta_c)L_b^2S+(\lambda_b+4\eta_b)L_b^2Q}+\frac{\left(\frac{4T}{e^2}+(4\lambda_c-6)L_b^2S+4\eta_bL_b^2Q\right)(3-2\lambda_c)L_b^2S}{\frac{4T}{e^2}+4(\lambda_c+\eta_c)L_b^2S+(\lambda_b+4\eta_b)L_b^2Q}\right]}{\left[\left(\frac{4T}{e^2}+4\lambda_cL_b^2S+4L_b^2\eta_bQ\right)-\frac{\left(\frac{4T}{e^2}+(4\lambda_c-6)L_b^2S+4\eta_bL_b^2Q\right)^2}{\frac{8T}{e^2}+8(\lambda_c-\eta_c)L_b^2S+(2\lambda_b+8\eta_b)L_b^2Q}-\frac{\left(\frac{4T}{e^2}+(4\lambda_c-6)L_b^2S+4\eta_bL_b^2Q\right)^2}{\frac{8T}{e^2}+8(\lambda_c+\eta_c)L_b^2S+(2\lambda_b+8\eta_b)L_b^2Q}\right]} \tag{67}
$$

$$
a_1=\frac{\left(\frac{4T}{e^2}+4\lambda_cL_b^2S+4\eta_bL_b^2Q\right)-\frac{\left(\frac{4T}{e^2}+(4\lambda_c-6)L_b^2S+4\eta_bL_b^2Q\right)^2}{\frac{4T}{e^2}+4(\lambda_c+\eta_c)L_b^2S+(\lambda_b+4\eta_b)L_b^2Q}\frac{e}{2}}{\left(\frac{4T}{e^2}+4\lambda_cL_b^2S+4L_b^2\eta_bQ\right)-\frac{2\left(\frac{4T}{e^2}+(4\lambda_c-6)L_b^2S+4\eta_bL_b^2Q\right)^2}{\frac{8T}{e^2}+8(\lambda_c+\eta_c)L_b^2S+(2\lambda_b+8\eta_b)L_b^2Q}}=\frac{e}{2} \tag{68}
$$

Eqs. (64) and (65) can be rewritten using Eq. (68) as follows:

$$
\frac{M_{AB}}{L_b}=a_2P \tag{69}
$$

$$
\frac{M_{DC}}{L_b}=a_3P \tag{70}
$$

Where

$$
a_2=\frac{2T-4\eta_cL_c^2S+2\eta_bL_c^2Q}{8T+8(\lambda_c-\eta_c)L_c^2S+(2\lambda_b+8\eta_b)L_c^2Q}e \tag{71}
$$

As a result:

$$
a_3=\frac{2T+2\eta_bL_c^2Q}{8T+8(\lambda_c+\eta_c)L_c^2S+(2\lambda_b+8\eta_b)L_c^2Q}e \tag{72}
$$

As it was mentioned before, using small amounts for η_b and η_c, the assumption of $a_2\approx a_3$ could be a good approximation. Of course, the assumption was proved to be very satisfactory in numerical calculations.

$$
\frac{1}{2}-2\frac{a_3}{e}=\frac{4(\lambda_c+\eta_c)L_c^2S+\lambda_bL_c^2Q}{8T+8(\lambda_c+\eta_c)L_c^2S+(2\lambda_b+8\eta_b)L_c^2Q} \tag{73}
$$

To figure out total strain energy in the main structure ($U_T=2U$), Eqs. (68), (69) and (70) need to be supplanted,

leading to Eq. (74) as follows:

$$U_T = 2P^2T\left[2\left(\frac{1}{2}-2\frac{a_3}{e}\right)^2\right]+ 2P^2L_c^2S\left[8\lambda_c\left(\frac{a_3^2}{e^2}\right)-2\eta_c\left(\frac{1}{2}-2\frac{a_3}{e}\right)\right]+ 2P^2L_c^2Q\left[2\lambda_b\left(\frac{a_3^2}{e^2}\right)+2\eta_b\left(\frac{1}{2}-2\frac{a_3}{e}\right)^2\right] \quad (74)$$

To calculate the elastic lateral stiffness of the EBMRF subjected to lateral load, the value of Δ_{C_x} needs to be calculated first. Using Castigliano's second theorem and Eq. (74), the value of Δ_{C_x} is calculated by Eq. (75) as follows:

$$\Delta_{C_x} = \frac{\partial U_T}{\partial P} = \left[(8T+8\eta_bL_c^2Q)\left(\frac{1}{2}-2\frac{a_3}{e}\right)^2+ (32\lambda_cL_c^2S+8\lambda_bL_c^2Q)\left(\frac{a_3^2}{e^2}\right)- 8\eta_cL_c^2S\left(\frac{1}{2}-2\frac{a_3}{e}\right)\right]P \quad (75)$$

The elastic lateral stiffness of the EBMRF subjected to lateral load P is calculated by Eq. (76) and simplified by Eq. (72) as follows:

$$K = \frac{P}{\Delta_{C_x}} = \frac{1}{(8T+8\eta_bL_c^2Q)\left(\frac{1}{2}-2\frac{a_3}{e}\right)^2+(32\lambda_cL_c^2S+8\lambda_bL_c^2Q)\left(\frac{a_3^2}{e^2}\right)-8\eta_cL_c^2S\left(\frac{1}{2}-2\frac{a_3}{e}\right)} \quad (76)$$

After placing a_3 in Eq. (75), the lateral stiffness of EBMRF subjected to lateral load P is calculated using Eq. (77) as below:

$$K = \frac{P}{\Delta_{C_x}} = \frac{(8T+8(\lambda_c+\eta_c)L_c^2S+(2\lambda_b+8\eta_b)L_c^2Q)^2}{[4(2T+2\eta_bL_c^2Q)(4(\lambda_c+\eta_c)L_c^2S+\lambda_bL_c^2Q)^2+8(4\lambda_cL_c^2S+\lambda_bL_c^2Q)(2T+2\eta_bL_c^2Q)^2-8\eta_cL_c^2S(4(\lambda_c+\eta_c)L_c^2S+\lambda_bL_c^2Q)(8T+8(\lambda_c+\eta_c)L_c^2S+(2\lambda_b+8\eta_b)L_c^2Q)]} \quad (77)$$

The Eq. (77) could be simplified and rewritten as follows:

$$K = \frac{P}{\Delta_{C_x}} = \frac{(8T+8\lambda_cL_c^2S+(2\lambda_b+8\eta_b)L_c^2Q)^2}{[4(2T+2\eta_bL_c^2Q)(4\lambda_cL_c^2S+\lambda_bL_c^2Q)^2+8(4\lambda_cL_c^2S+\lambda_bL_c^2Q)(2T+2\eta_bL_c^2Q)^2-8\eta_cL_c^2S(4\lambda_cL_c^2S+\lambda_bL_c^2Q)(8T+8\lambda_cL_c^2S+(2\lambda_b+8\eta_b)L_c^2Q)]} \quad (78)$$
$$\rightarrow K = \frac{2(4T+4\eta_bL_c^2Q+4\lambda_cL_c^2S+\lambda_bL_c^2Q)}{(4\lambda_cL_c^2S+\lambda_bL_c^2Q)(4T+4\eta_bL_c^2Q-8\eta_cL_c^2S)}$$

The stiffness equation can be simplified as follows, neglecting η_c as compared to λ_c.

$$K = \frac{P}{\Delta_{C_x}} = \frac{(8T+8\lambda_cL_c^2S+(2\lambda_b+8\eta_b)L_c^2Q)^2}{[4(2T+2\eta_bL_c^2Q)(4\lambda_cL_c^2S+\lambda_bL_c^2Q)^2+8(4\lambda_cL_c^2S+\lambda_bL_c^2Q)(2T+2\eta_bL_c^2Q)^2-8\eta_cL_c^2S(4\lambda_cL_c^2S+\lambda_bL_c^2Q)(8T+8\lambda_cL_c^2S+(2\lambda_b+8\eta_b)L_c^2Q)]} \quad (78)$$
$$\rightarrow K = \frac{2(4T+4\eta_bL_c^2Q+4\lambda_cL_c^2S+\lambda_bL_c^2Q)}{(4\lambda_cL_c^2S+\lambda_bL_c^2Q)(4T+4\eta_bL_c^2Q-8\eta_cL_c^2S)}$$

The stiffness equation can be simplified as follows, neglecting η_c as compared to λ_c.

Finally, by incorporating Eqs. (52), (53) and (54) into Eq. (77), the lateral stiffness of the EBMRF subjected to lateral load P is calculated using Eq. (80) as follows:

$$\frac{K}{\frac{EA_e}{L_b}} = \frac{2}{\left(\Psi_{bav}+\frac{\eta_be^2}{3\gamma}-\frac{\eta_c\beta e^3}{6\gamma}\right)}+ \frac{24\gamma}{(\lambda_be^2+\lambda_c\beta e^3)\left(1-\frac{\frac{\eta_c\beta e^2}{6\gamma}}{\Psi_{bav}+\frac{\eta_be^2}{3\gamma}}\right)} \quad (80)$$

The normalized stiffness, $\phi(\gamma,\beta,e,\frac{h}{r_E},\alpha_s)$, can be defined as the ratio of lateral stiffness of the EBMRF system to the elliptic bracing stiffness as follows:

$$\frac{K}{\frac{EA_e}{L_b}} = \phi(\gamma,\beta,e,\frac{L_c}{r_e},\alpha_s) \quad (81)$$

where

$$\phi(\gamma,\beta,e,\frac{h}{r_E},\alpha_s) = \frac{12\gamma}{(6\gamma\psi_{bav}+2\eta_be^2-\eta_c\beta e^3)}+ \frac{24\gamma}{(\lambda_be^2+\lambda_c\beta e^3)\left(1-\frac{\eta_c\beta e^2}{6\gamma\psi_{bav}+2\eta_be^2}\right)} \quad (82)$$

The first term is the contribution of the steel moment frame and the second one is the contribution of the elliptic

$$K = \frac{1}{(2T+2\eta_bL_c^2Q-4\eta_cL_c^2S)}+\frac{2}{(4\lambda_cL_c^2S+\lambda_bL_c^2Q)\left(1-\frac{4\eta_cL_c^2S}{2T+2\eta_bL_c^2Q}\right)} \quad (79)$$

brace in Eq. (82). According to Eq. (82), if the stiffness of the brace is higher than that of the beam (is γ was small), and the stiffness of the beam is not much different from that of the column (is β was normal), the participation of the second term will be higher than the first one, and the normalized stiffness value (ϕ) can be considered equal to $\frac{2}{\psi_{bav}}$. This approximation can be usually carried out in engineering structures. On the other hand, it should be noted that by considering a small value for γ and a large value for β, the lateral stiffness equation for the EBMRF can be obtained using Eq. (82).

Finally, the elastic lateral stiffness of the EBMRF subjected to the lateral force (P) can be calculated by an improved and innovative relation through the strain energy method based on the geometric properties of the employed sections and specifications of the utilized material as follows:

1. Calculate e by dividing the column length to beam length (Eq. (1)).
2. Calculate β by dividing the moment of inertia of the beam to that of the column (Eq. (55)).
3. Calculate γ (Eq. (56)).
4. Calculate$\lambda_c$and η_c using $\frac{L_c}{r_c}$, α_c and e (Eq. (53)).
5. Calculate$\lambda_b$and η_b using $\frac{L_b}{r_b}$,α_b and e (Eq. (54)).
6. Calculate the parameter $\Psi_{bav}(e)$ for different values of e (Eq. (49) or Fig. 8).
7. Calculate the normalized stiffness (ϕ) (Eq. (79)).
8. Calculate the elastic lateral stiffness of EBMRF (Eq. (80)).

2.3 Special cases of elastic stiffness in EBMRF system

The elastic stiffness of a steel moment frame with a two dimensional one-story one-span elliptic brace with rigid connections under the lateral load of P in roof level considering the effects of all of the deformations due to the axial and shear forces and bending moments in beams, columns and the elliptic brace can be calculated using Eq. (79).

If the effects due to the deformations caused by axial and shear forces were neglected in beams and columns, the elastic stiffness of a moment steel frame with a two dimensional one-story one-span elliptic brace under the lateral load of P in roof level would be simplified as below by adding lateral stiffness of moment frame and elliptic brace.

$$K = \frac{24}{e^2 + e^3 \frac{I_b}{I_c}} \frac{EI_b}{L_b^3} + \frac{2}{\psi_{bav}} \frac{EA_e}{L_b} \tag{83}$$

The difference between the amounts of elastic stiffness of a two dimensional one-story one-span steel moment frame and an elliptic frame with rigid connections under the lateral load of P considering the effects of the deformations due to axial and shear forces in beams and columns (Eq. (79)) and without considering those (Eq. (83)) is about three percent. Since the effects of the deformations due to axial and shear forces in beams and columns are usually neglected in studies, the simplified Eq. 83 could be used as a proper equation to calculate elastic stiffness of a two dimensional one-story one-span steel moment frame with an elliptic brace and with rigid connections subjected to the lateral load of P. The below-mentioned special cases could be evaluated.

Case 1) A rigid beam

1.a) A single story frame with n_1 spans and elliptic braces in n_2 spans are considered here. If the beam was considered as a rigid element with an infinite flexural rigidity, the elastic stiffness of steel moment frame with an elliptic brace under the lateral load of P in roof level could be exactly and explicitly calculated as follows. The support of both columns are fixed. Therefore, in this special case, each column will behave as a beam with a fixed support at one end and a sliding support at the other end with a translational stiffness of $\frac{12EI_c}{{L_c}^3}$. In this case, the lateral force is distributed between the columns of the frame and its elliptic braces. The displacement of the columns and the braces will be the same, showing that columns and elliptic braces behave as parallel springs; therefore, the stiffnesses of the springs are summed. In this frame with n_1 spans, there are $n_1 + 1$ columns. Therefore,

$$K = (n_1 + 1)\left(\frac{12EI_c}{{L_c}^3}\right) + n_2\left(\frac{2}{\psi_{bav}} \frac{EA_e}{L_b}\right) \tag{84}$$

1.b) The elastic stiffness of a two-dimensional frame with n_1 spans and the elliptic braces installed in n_2 spans was calculated by Eq. (84). In this case, the frame has n_3 stories and the lateral force of P in roof level is tolerated all stories, and the lateral relative deformations of the stories (drift) are summed and resulted in the roof displacement. With this explanation, the equivalent lateral stiffness of different stories of the structure are combined as series springs. The equivalent stiffness of the set of n springs which combined in series manner, equals $\frac{K}{n}$.

A n_3- story frame with n_1 spans is considered. The number of the spans with an elliptic brace is assumed n_2. If the beams were rigid, the flexural rigidity of the beams would tend to infinity. If the lateral load P was applied in the roof level, the elastic stiffness could be exactly and explicitly calculated as follows:

$$K = \frac{1}{n_3}\left[(n_1 + 1)\left(\frac{12EI_c}{{L_c}^3}\right) + n_2\left(\frac{2}{\psi_{bav}} \frac{EA_e}{L_b}\right)\right] \tag{85}$$

Case 2) An elastic beam

2.a) A single story, with n_1 spans frame, n_2 spans of which with elliptic braces is considered. If the beam was considered as an elastic element, moreover, if the number of the spans of the frame was assumed as 2^N $(n_1 = 2^N)$, and the flexural rigidity of the middle columns was two times

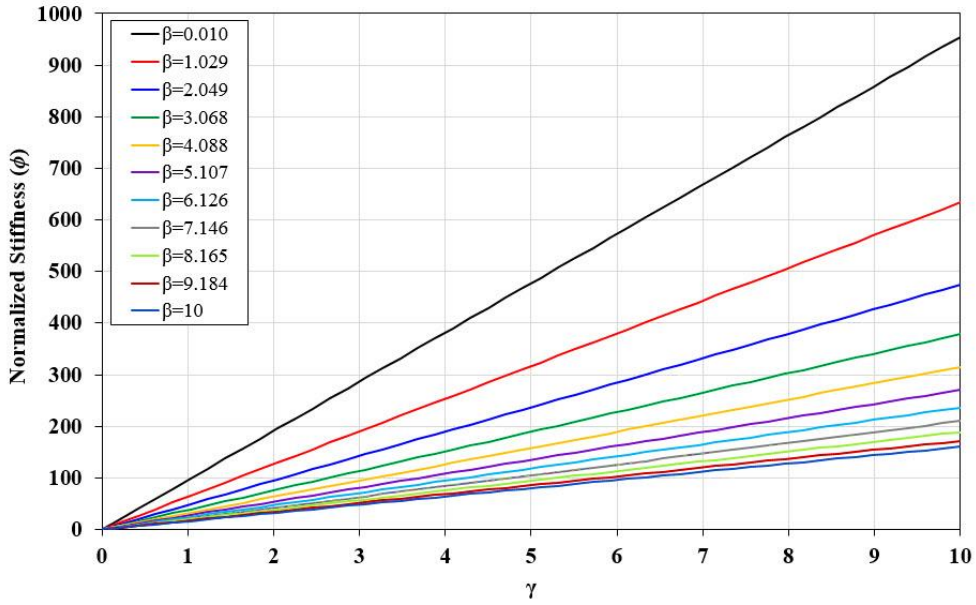

Fig. 9 Changes in normalized stiffness,ϕ, versus parameter γ for different values of β based on numerical models

the other columns, the elastic stiffness of the bending moment with an elliptic brace under the lateral load of P in the roof

$$K = n_1\left(\frac{24}{e^2 + e^3\frac{I_b}{I_c}}\frac{EI_b}{L_b^3}\right) + n_2\left(\frac{2}{\psi_{bav}}\frac{EA_e}{L_b}\right) \quad (86)$$

In this case, the stiffness of the different frames and the elliptic braces are summed. In other words, they act as parallel springs. The frame could be decomposed in n_1 separate spans and the stiffness of the frame could be assumed as n_1 times the stiffness of one span considering the two above-mentioned assumptions as well as the rules govern the axially symmetric structures subjected to antisymmetric loadings.

3. Numerical OpenSees Modeling and Verification

OpenSees 2.4.6 software (2013) was employed in modeling and conducting the analysis of the two-dimensional single-story single-span steel moment frames equipped with an elliptic brace under the lateral load. To model the elements of the braced frame within a linear deformation range, the following assumptions are made:

(1) The elastic beam-column elements are adopted to model the beams, columns and the elliptic brace.
(2) The beams and the columns are divided into two equal parts to determine the connection point of the elliptic brace to the elements of beam and column.
(3) To enhance accuracy of the analysis, each quarter elliptic brace is divided into 10 parts with equal length *dx*.
(4) Two equal and antisymmetric lateral forces of 5000 N are applied to each of the upper nodes of the two-dimensional frame.
(5) The two-dimensional structures and lateral forces are considered in an *xz* plane and the degrees of freedom for all the nodes, except for those of the bracing, are rigid in the *y* direction.
(6) Rigid beam-to-column connections are considered.
(7) The connection of the elliptic brace to the middle points of the beams and columns is considered as a hinge using the zero-length element.
(8) The uniaxial elastic material is assigned for the beam and columns.
(9) In this modeling, the effect of linear geometric transformation is considered.
(10) In the finite element analysis, the effects of the geometric nonlinearities are ignored because of the theoretical premises adopted in calculating the elastic drift of the frames.

The finite element analysis using OpenSees software (2013) is performed so as to evaluate the reliability and accuracy of Eq. (81). To this end, 2500 single-story, single-span SEM-ELs under two equal and anti-symmetric lateral forces of $\frac{P}{2}$ applied to the two upper nodes of the frame, each of which is equal to 5000 *N*, are modeled. The story height and span length (centerline to centerline distance) for the EBMRFs are equal to 4000 *mm* and 8000 *mm*, respectively. The cross-sectional area (A_e) and the moment of inertia of the elliptic brace about the bending axis (strong axis), I_e, are 10^5 mm^2 and 6.4×10^8 mm^4, respectively. The slenderness ratio of the elliptic brace $(L_c/r_e)$and the aspect ratio of the elliptic-braced frame (e) are 50 and 0.5, respectively. For the geometry of the elliptic-braced frame with 50 different values of bending stiffness ratio of the beam to the elliptic brace (γ) and 50 different values of bending stiffness ratio of the beam to the column (β), the values of the moment of inertia for the beam (I_b) and the column (I_c) about the bending axis can be calculated by Eqs. (57) and (54), respectively. All known parameters are defined using MATLAB programming code and assigned to

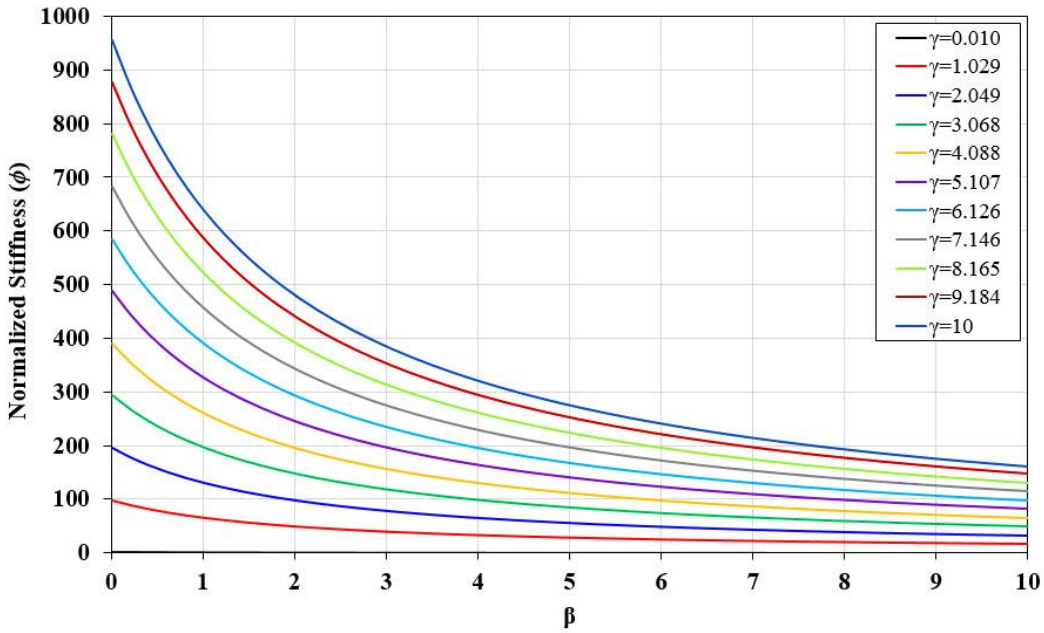

Fig. 10 Changes in normalized stiffness,ϕ, versus parameter β for different values of γ based on numerical models

numerical models in OpenSees software. The numerical models are implemented in OpenSees software and the lateral displacement for one of the upper nodes is recorded. Then the elastic lateral stiffness of the EBMRFs is calculated by dividing the lateral force of 10000 *N* by the lateral displacement of the elliptic-braced frame

Fig. 9 shows the diagrams for the changes in normalized stiffness of the SFM-EL system with different flexural stiffness ratios of beam to elliptic bracing $(\phi - \gamma)$. The $\phi - \gamma$ graphs are drawn with constant elliptic bracing slenderness ratio (L_c/r_e) equal to 50, the shear shape coefficient (α_s) equal to zero and the aspect ratio of the frame (e) equal to 0.5 for 50 different values of the flexural stiffness ratio of the beam to the elliptic brace (γ) ranging from 0.01 to 10 and 50 different values of the moment of inertia ratio of the beam to the column (β) between 0.01 and 10. To better illustration the graphs, only 11 values from 50 values between 0.01 and 10 are selected for β. Interpolation can be done for intermediate values. The reason behind disregarding the shear shape coefficient (α_s) in numerical models is that OpenSees finite element software is capable of considering the shear effects in the analysis. For this reason, in this section, the numerical models are validated through the analytical equation by assuming the value of α_s equal to zero. According to Eq. (82), it can be observed that the normalized stiffness of the SFM-EL system is a linear function of β and increases with an increase in γ. Using this mode, the normalized diagrams of the stiffness change (ϕ) with the parameter γ for different values of β should be normally linear and start from zero.

Fig. 10 shows diagrams for the changes in normalized stiffness of the SFM-EL system for different beam-to-column ratios of moment of inertia$(\phi - \beta)$. The $(\phi - \beta)$diagrams are obtained with constant elliptic bracing slenderness ratio (L_c/r_e)equal to 50, the shear shape coefficient (α_s) equal to zero and the aspect ratio of the frame (e) equal to 0.5 for 50 different flexural stiffness ratios of the beam to the elliptic brace (γ) between 0.01 and 10 and 50 different moment of inertia ratios of the beam to the column (β) between 0.01 and 10. To distinguish the graphs, only 11 values of γ were selected from 50 values between 0.01 and 10, and the graphs were plotted, and interpolation could be used for intermediate values. In this section, the numerical models are validated by the analytical equation assuming that the value of α_s equals zero. According to Eq. (82), the effect of the parameter β on the normalized stiffness of the SFM-EL system is harmonic, and the normalized stiffness decreases with any increase in β.

The theoretical equation to calculate the stiffness will be simplified by neglecting the shear effect in the beams and columns $(\eta_b = 0\text{and } \eta_c = 0)$. The results of the equation will be comparable to those of the finite element models.

$$\phi(\gamma, \beta, e, \frac{h}{r_E}, \alpha_s) = \frac{2}{\psi_{bav}} + \frac{24\gamma}{(\lambda_b e^2 + \lambda_c \beta e^3)} \quad (87)$$

In Fig. 11, for a given value of γ, the constant slenderness ratio of the elliptic brace (L_c/r_e)equal to 50, the shear shape coefficient (α_s) equal to zero and the aspect ratio of the frame (e) equal to 0.5, the values of the computational parameter(ϕ) from the numerical models with different amounts of γ are completely consistent with those obtained by Eq. (82), which in turn, indicates complete consistency of the proposed relationship with the numerical models. The $\phi - \beta$ diagram is depicted in Fig. 11.

A fixed value of $\beta(\beta = 4.901)$ and the constant slenderness ratio of the elliptic brace $(L_c/r_e = 50)$, the zero shear shape coefficient $(\alpha_s = 0)$ and the constant aspect ratio of the frame $(e = 0.5)$ are assumed to calculate the parameterϕ, the picket in Fig. 12. Regarding the linear variation of the normalized stiffness (ϕ) in term of γ align is fitted to the carve.

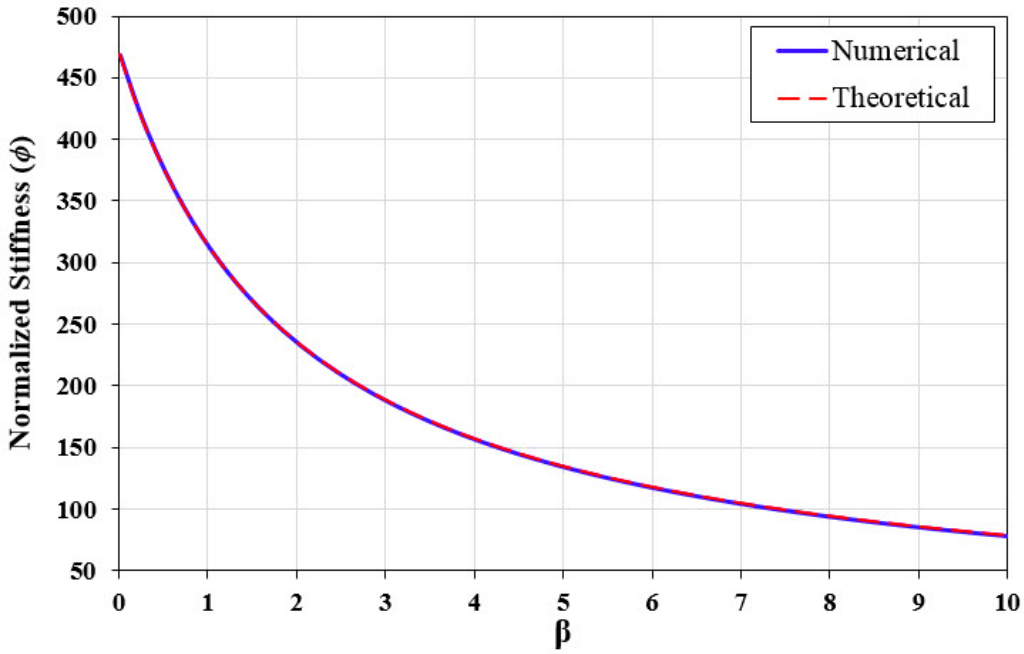

Fig. 11 The comparison of the results from the numerical models and Eq. (82) for normalized stiffness changes(ϕ) versus parameter β assuming constant $\gamma = 4.901$

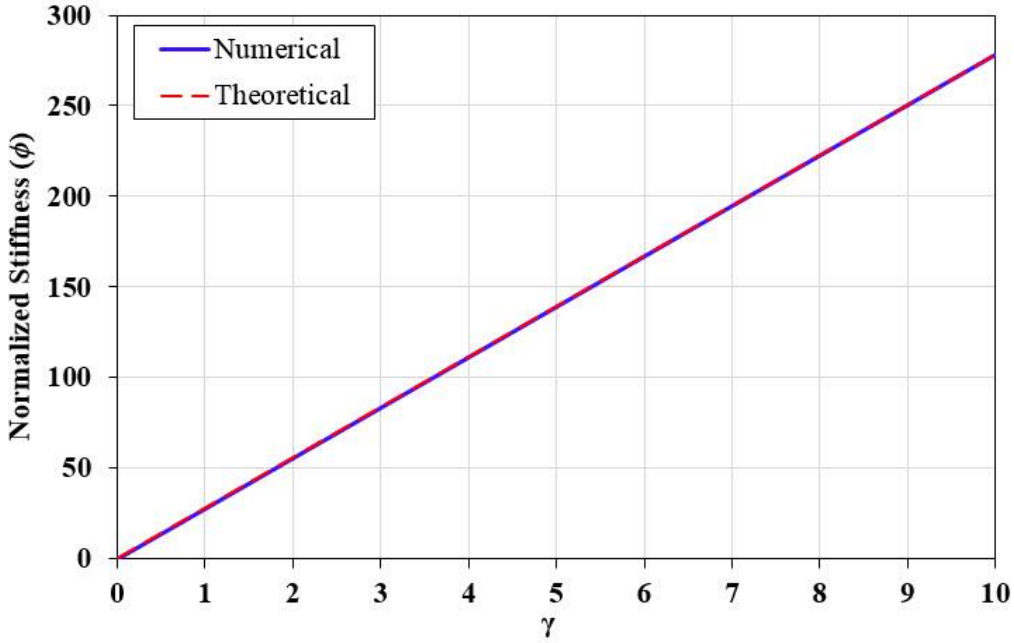

Fig. 12 The comparison of the results obtained from the numerical models and Eq. (82) for normalized stiffness changes (ϕ) versus parameter γ assuming constant $\beta = 4.901$

4. The equivalent Element for the Elliptic-Braced Element

4.1 Calculation of the elastic axial stiffness of the equivalent element for the elliptic-braced element

To account for the overall strength and elastic axial stiffness of the EBMRF, an equivalent simple linear element is used, which transmits the force to the middle points of the beams and columns. This modeling leads to a marked reduction in the number of elements constituting the elliptic brace. Details of the EBMRF and schematics of the equivalent element model are presented in Fig. 13.

The strain energy of each quarter elliptic brace is calculated by Eq. (45). Incorporating Eq. (1) into Eq. (45) results in the constituent terms of Eq. (45) as follows:

$$U_{elliptic\ \ brace,bav} = \frac{F^2 L_b}{4EA_e}\frac{\Psi_{bav}}{1+e^2} \tag{88}$$

By differentiating the strain energy with respect to the

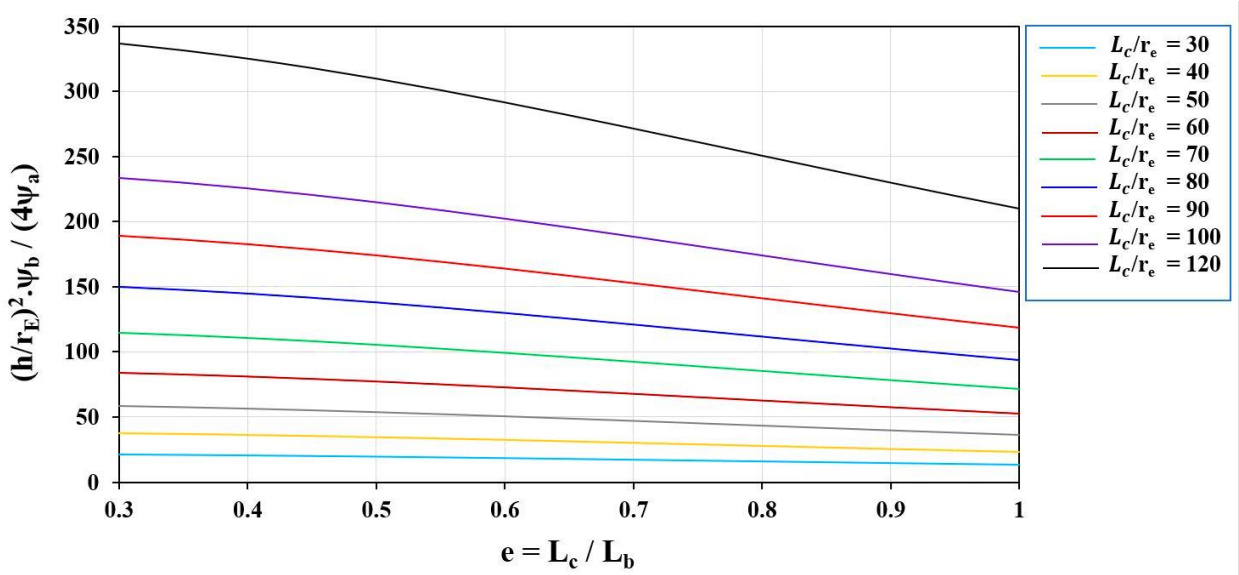

Fig. 14 Term changes of strain energy due to bending moment participation relative to strain energy due to axial force versus parameter e

axial force F, the increase in the equivalent spring length can be calculated by Eq. (89):

$$\Delta = \frac{\partial U}{\partial F} = \frac{FL_b}{2EA_e}\frac{\Psi_{bav}}{1+e^2} \tag{89}$$

The stiffness of the linear spring (K) for a structure is a measure of the resistance offered by an elastic structure against deformation. For an elastic structure with a Single Degree Of Freedom (SDOF), stretching or compressing of a rod, the stiffness is defined as $K=F/\Delta$, where F denotes the force on the structure and Δ presents the deformation. The equivalent spring stiffness for each quarter elliptic brace is calculated by Eq. (90).

$$K = \frac{F}{\Delta} = \frac{2EA_e}{L_b\frac{\Psi_{bav}}{1+e^2}} \tag{90}$$

The parameter $\Psi_{bav}(e)$ is calculated using Eq. (48) or Eq. (56) and is only a function of the parameter$e$; therefore, it can be numerically solved. The value of $\Psi_{bav}(e)$ for different values of e is illustrated in Fig. 8. Given that the normalized stiffness is defined as the ratio of the axial rigidity of the elliptic brace to the beam length,$\frac{EA_e}{L_b}$, the normalized stiffness for each of the equivalent spring elements of the quarter elliptic brace can be defined by Eq. (91) as follows:

$$\frac{K}{\frac{EA_e}{L_b}} = \frac{2}{\Psi_{bav}}(1+e^2) \tag{91}$$

4.2 The effects of strain energy of bending moment, shear and axial forces on the amount of lateral stiffness of the elliptic brace

The objective of this section is to determine the amount of contribution of each internal action in the strain energy.

In this regard, bending moment, shear and axial forces are considered for calculating the elastic lateral stiffness of the equivalent element for the elliptic brace. The elastic lateral stiffness is obtained by a quarter elliptic brace from Eq. (92) as follows:

$$\phi = \frac{2}{\Psi_{bav}}(1+e^2) = \frac{2}{\left(\frac{L_c}{r_e}\right)^2\frac{\Psi_b}{4} + 2.6\alpha_s\Psi_v + \Psi_a} \tag{92}$$

As Eq. (92) shows, all of the three effects of axial force, shear force and bending moment are located on the denominator of the fraction. Therefore, the lowest value of Ψ will have the greatest effect on the total elastic stiffness. Accordingly, Eq. (92) can be rewritten as follows:

$$\frac{1}{\phi} = \frac{\Psi_a}{2}\left[\left(\frac{L_c}{r_e}\right)^2\frac{\Psi_b}{4\Psi_a} + \frac{2.6\alpha_s\Psi_v}{\Psi_a} + 1\right] \tag{93}$$

Each of the terms $\frac{\Psi_b}{4\Psi_a}$ and $\frac{2.6(\alpha_s)\Psi_v}{\Psi_a}$ can be plotted as a function of the parameter e. The contribution of bending moment in the total strain energy in much greater than those of axial and shear forces, as shown in Figs. 14 and 15. demonstrate that the effect of the expression for bending moment energy.

5. Numerical Example for the Calculation of Stiffness

5.1 Calculation of elastic stiffness in a two-dimensional single-story single-span EBMRF

In this section, the developed equations are validated in the calculation of elastic lateral stiffness of a steel moment frame equipped with an elliptic brace. In this regard, a single-story single-span frame equipped with elliptic bracing in SAP software.

The quality of the results is evaluated by comparing the outcomes of a finite element analysis to those of the

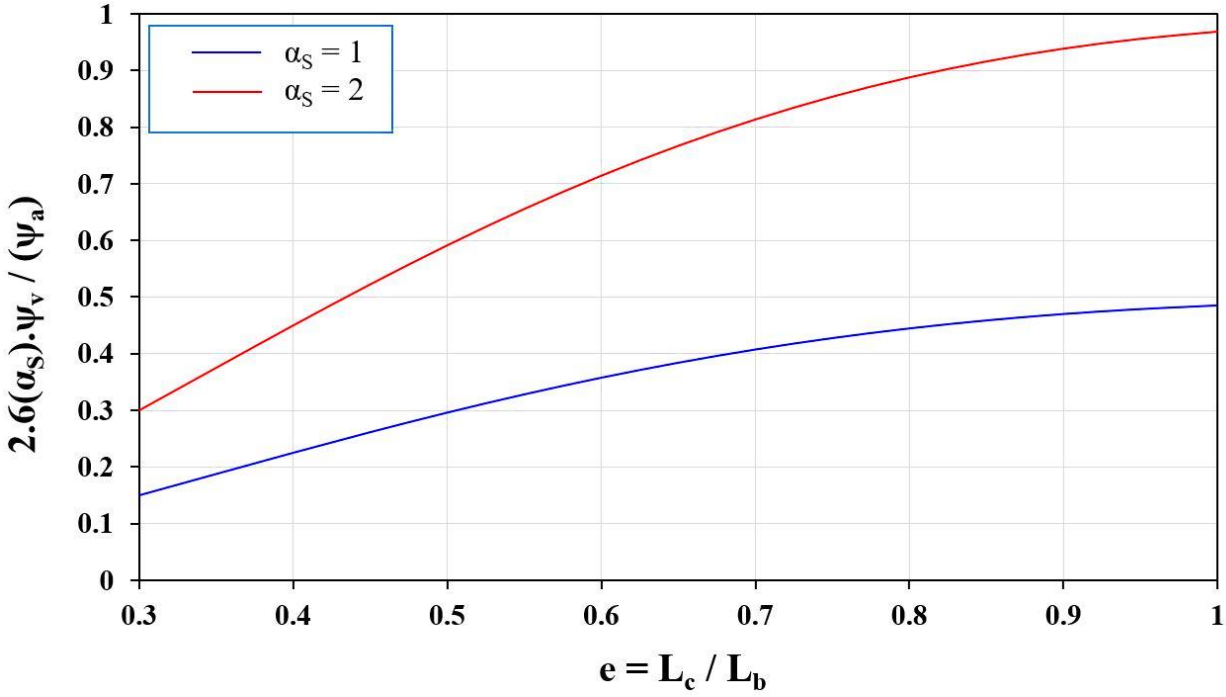

Fig. 15 Term changes of strain energy due to shear force participation relative to strain energy due to axial force versu sparameter e

proposed elastic lateral stiffness formulation for a two-dimensional single-story single-span EBMRF.

The quality of the results is evaluated by comparing the outcomes of an analysis by the SAP2000 software and those of the proposed elastic lateral stiffness formulation for a two-dimensional single-story single-span EBMRF. This example is used to illustrate the design method described in section 3.

The studied problem consists of a single-story single-span steel moment frame with rigid beam-to-column connections equipped with an elliptic brace (EBMRF). The connection of four quadruple elliptic braces to each other is made by hinges. Each quarter elliptic brace is divided into 10 parts to increase the accuracy of the analysis. The connection of four quadruple elliptic braces to each other is made by hinges. Each quarter elliptic brace is divided into 10 parts to increase the accuracy of the analysis.

The ratio of the length to the height (e) is chosen equal to 0.8, which results in the values of 5000 *mm* and 4000 *mm* for the beam length and column length (distances between centerlines) of EBMRF, respectively. Boundary elements, including beams and columns of the I-shape profile with the specifications of outside height, flange width, flange thickness and web thickness are considered equal to 300, 150, 10 and 6 *mm*, respectively. The moment of inertia of the beam and column elements about the bending axis (strong axis) is equal to 74076000 mm^4. In the EBMRF bracing system, the cross-section of the elliptic brace is box-shape 100 × 6. The cross-section area of the elliptic brace is 2256 mm^2, and the radius of gyration and the slenderness ratio of the elliptic brace$(L_c/r_e)$are 38.45 *mm* and 104.022, respectively.

The shape coefficient (α_s) for the elliptic brace profile is equal to 2.0. Also, the elastic modulus of the utilized steel (E) is equal to 200,000 *MPa*. The structure, loading and seismic force on the *xz* plane are considered two-dimensional. Two equal and antisymmetric lateral forces, each equal to 5000 *N*, are applied to the two upper nodes *B* and *C* (Fig. 16).

The elastic lateral stiffness of the EBMRFs is calculated by dividing lateral force of 10000 *N* by the lateral displacement resulting from the finite element analysis.

$$K = \frac{P}{\Delta} = \frac{10000}{3.5327} = 2830.69 \frac{N}{mm} \tag{94}$$

The elastic lateral stiffness of the EBMRFs is calculated using the formulation proposed in this study and presented in Table 1.

The comparison of the obtained results from the finite element analysis and the proposed formulation of elastic lateral stiffness for a two-dimensional single-story single-span EBMRF (Eq. 81) shows the lack of suitable pure error of less than two percent. If the value of the shear shape coefficient was set to zero in the proposed formulation, it would be observed that the role of this coefficient in calculating the elastic lateral stiffness of the EBMRF would be very small and negligible.

5.2 The calculation of elastic stiffness for the equivalent linear spring element of a quarter elliptic brace

In this section, the developed equation is verified in the calculation of elastic lateral stiffness for a quarter elliptic brace. For this purpose, a linear spring element of a quarter elliptic brace is modelled in SAP software. The quality of the results is evaluated by comparing the outcomes of the finite element analysis and those of the proposed formulation for the

Table 1 The lateral stiffness of the elliptic-brace moment resisting frame (EBMRFs) using the proposed formulation

No.	Eq. or Fig. No.	Parameters	Calculated parameter(s)
1	Eq. 1	e	0.8
2	Eq. 55	β	1
3	Eq. 56	γ	0.001313
4	Eq. 53	η_c and λ_c	$\lambda_c = 1.019$ $\eta_c = 0.008$
5	Eq. 54	η_b and λ_b	$\lambda_b = 1.012$ $\eta_b = 0.003$
6	Eqs. (35), (39) and (43) or Fig.6	$\Psi_b(e)$,$\Psi_a(e)$ and $\Psi_v(e)$	$\Psi_b(e) = 0.077$ $\Psi_n(e) = 0.121$ $\Psi_v(e) = 0.124$
7	Eq. 48 or Eq. 49 or Fig. 8	$\Psi_{bav}(e)$	347.347
8	Eq. 82	$\phi(\gamma, \beta, e, \frac{L_c}{r_e}, \alpha_s)$	0.033
9	Eq. 80	K	$2830.79\frac{N}{mm}$

Table 2 The axial stiffness of the equivalent linear spring element from a quarter elliptic brace using the proposed formulation

No.	Equation and Fig. No.	Parameters	The calculated parameter(s)
1	Eq. 1	e	0.8
2	Eqs. (35), (39) and (43) or Fig.6	$\Psi_b(e)$,$\Psi_a(e)$ and $\Psi_v(e)$	$\Psi_b(e) = 0.077$ $\Psi_a(e) = 1.121$ $\Psi_v(e) = 0.124$
3	According to the geometric characteristics of the braced frame	$\frac{EA_e}{L_b}$	90240
4	Eq. 48 or Eq. 49 or Fig. 8	$\Psi_{bav}(e)$	346.124146
6	Eq. 91	K	$856.107\frac{N}{mm}$

elastic axial stiffness of the equivalent linear spring element.

The problem under study consists of a quarter elliptic brace, which supports the beginning and the end of the joint. The length to height ratio (e) is set to 0.8, giving the values for the length of the span and the height of the floor of an EBMRF (distances between centerlines) equal to 5000 *mm* and 4000 *mm*, respectively. The profile assigned for the quarter elliptic brace is Box-shape 100 × 6. The cross-sectional area of the elliptic brace is 2256 mm^2, and the radius of gyration and the slenderness ratio of the elliptic brace $(L_c/r_e)$are 38.45 mm and 104.022, respectively.

The shape coefficient (α_s) for elliptic bracing profiles is equal to 2.0. The elastic modulus of the utilized steel (E) is equal to 200,000 *MPa*. The structure and the load applied along the input line at the beginning and the end of the quarter elliptic brace on the xz plane are considered two-dimensional. A concentrated force of 1000 *N* along the input line at the beginning and the end of the quarter elliptic brace is applied to the upper node *C* (Fig. 17).

The elastic axial stiffness of an equivalent element for a quarter elliptic brace is calculated using the finite element analysis. For this purpose, the concentrated force equal to 1000 *N* along the input line at the beginning and the end of the quarter elliptic brace is divided by the displacement along with the force as follows:

$$K = \frac{P}{\Delta} = \frac{1000}{1.1669} = 856.971\frac{N}{mm} \quad (95)$$

The elastic axial stiffness of the equivalent spring element for a quarter elliptic brace is calculated using the formulation proposed in Table 2.

A comparison between the results obtained from the finite element analysis for a quarter elliptic brace and those by the formulation provided for an equivalent spring element of a quarter elliptic brace (Eq. (89)) results in a very small relative error (less than 1%).

If the value of the shear shape coefficient (α_s) in the proposed formulation was set to zero, it would be observed that the role of this coefficient would be very small and negligible in calculating the elastic axial stiffness of the equivalent spring element for an elliptic brace.

6. Elliptical bracing system and its comparison with other types of braces

The elliptic-braced frames as a new lateral braced system, when installed in the middle bay of the frames in the facade of a building, not only causes any problem to the opening space of the facade, but also improves the

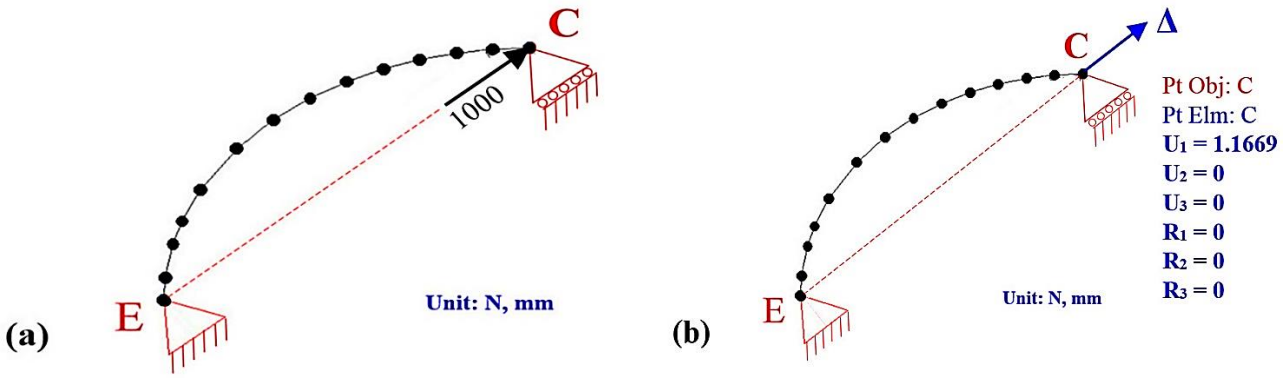

Fig. 17 (a) Two-dimensional modeling of a quarter elliptic brace with a simple two-headed end under the effect of a concentrated force along the input line at the beginning and the end of the quarter elliptic brace equal to 1000 N (b) elastic displacement at the same direction of the force.

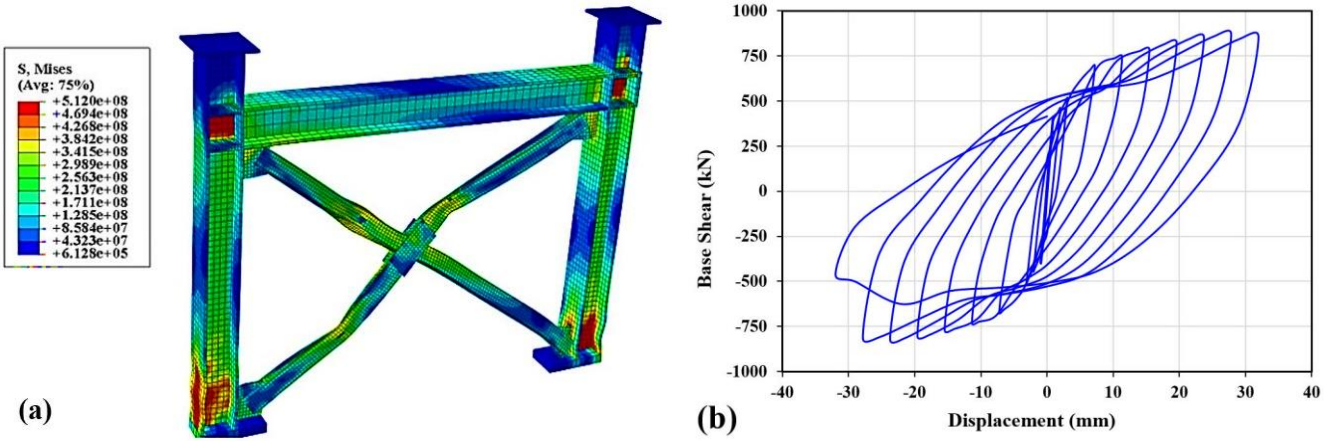

Fig. 18 (a) The von-Mises stress (Pa) in the X-braced frame at the final load step, 32 *mm* displacement, equal with 2.1% drift, and (b) hysteretic behavior

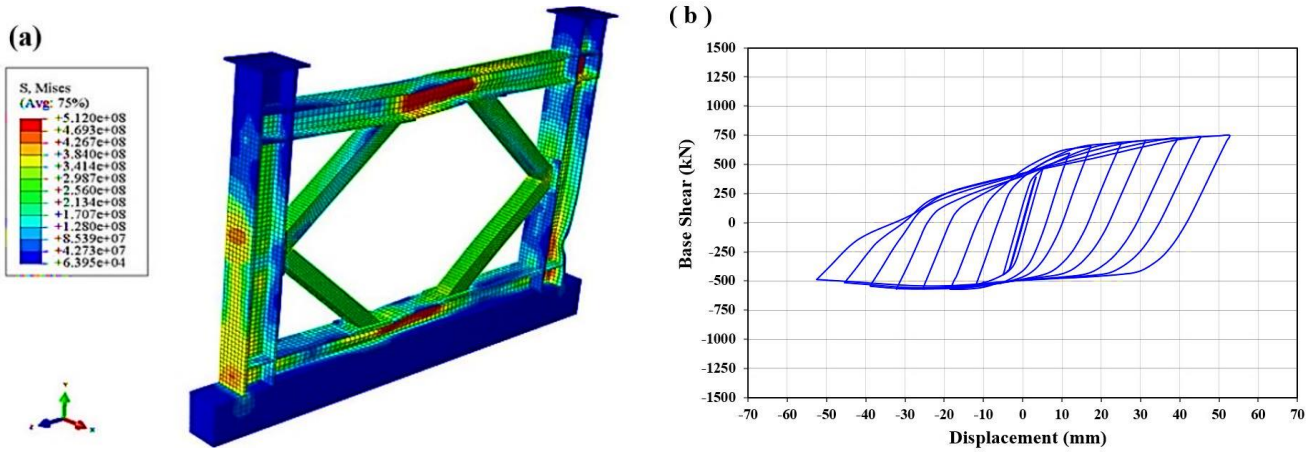

Fig. 19 (a) The von-Mises stress (Pa) in the K-braced frame at the final load step, 50 *mm* displacement, equal with 3.2% drift, and (b) hysteretic behavior

structural behavior. In recent studies, the authors have investigated several studies on the seismic performance of elliptic-braced frames (Ghasemi *et al*. 2016, 2019, 2020, 2021 and 2022). In one of the studies, Ghasemi *et al*. (2020 and 2021) evaluated the seismic behavior, energy absorption capacity, and global- and local-type failure mechanisms of a ½ scale single-story single-span elliptic-braced moment resisting frame (ELBRF) under cyclic quasi-static loading through experimental and analytical studies, and compared its result with the other types of braces such as X-, K- and Diamond-bracing systems in a story base model.

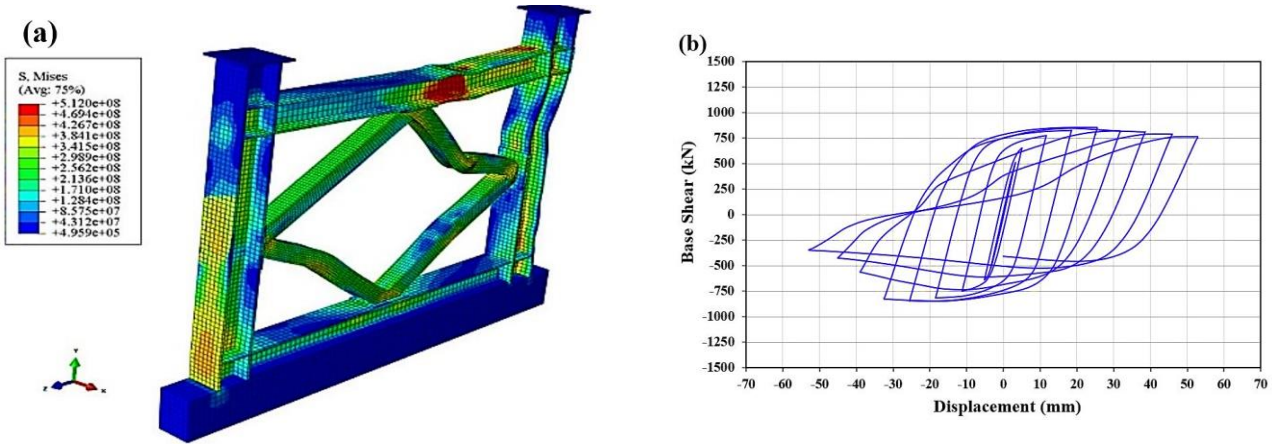

Fig. 20 (a) The von-Mises stress (Pa) in the Diamond-braced frame at the final load step, 54 *mm* displacement, equal with 3.2% drift, and (b) hysteretic behavior

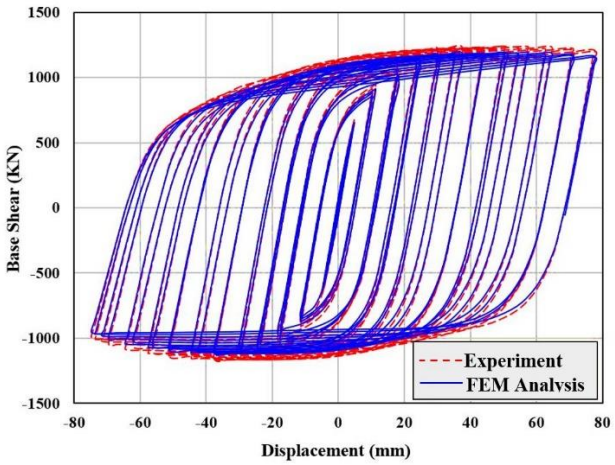

Fig. 21. The hysteresis behavior in the experimental and FEM analyses of the Elliptic-braced frame

Observations and output of the X-bracing finite element model revealed that the behavior mechanism of the system was shear failure. Out-of-plane sudden buckling of the bracing member in X-bracing caused damage to gusset plate, middle connection, and significant loss in structural strength and energy dissipation of the structure. The relatively small post-yield capacity and the brittle failure mode of the X-braced frame made this system inappropriate for a ductile design. It should be noted that despite the increase in the stiffness of the X-braced frame, the ductility and energy absorption capacity of the system reduced, Fig. 18.

The K-brace and diagonal members of the diamond brace are connected to the columns at the mid-height. The use of K-bracing and diamond brace has been prevented in seismic regions because of the high potential for the failure of columns when the compression braces undergo buckling. Output of the finite element model for the K- and diamond-braced systems indicated that the axial force was directly transmitted from the braces to the columns and with buckling of the compression brace, it immediately caused column failure. In these structural systems, energy absorption is low. In the K-braced and diamond-braced frames, buckling of the bracing member due to the cyclic behavior of the structure tightened the hysteresis loops, resulting in their poor energy absorption performance. Also, pinching effects were observed in the K-braced and diamond-braced frames, Figs. 19 and 20

Observation of the experimental studies and finite element model of the proposed ELBRF bracing system indicates that as the lateral force increased, plastic hinges occurred first at the elliptic brace, then at both ends of the beam, and finally at both ends of the column in the final steps of loading. In ELBRF bracing system, the lack of buckling of the columns and out-of-plane buckling of the elliptic brace is evident in all stages of cyclic loading.

In the ELBRF system, against to X-bracing, K-bracing, and diamond-bracing systems, there is a considerable difference between the drift corresponded to the first yield and ultimate drift resistance and the maximum relative deformation after entering the plastic zone, which leads to a strength degradation. Also, there exists a great interval between the formation of the first plastic hinge and the collapse time of the structure. Considering the formation of plastic hinges in ELBRF frames, it was found out that, first, the elliptic brace entered the plastic deformation, reached results in energy dissipation. Then, plastic structure hinges occurred at both ends of the beam and finally, they reached

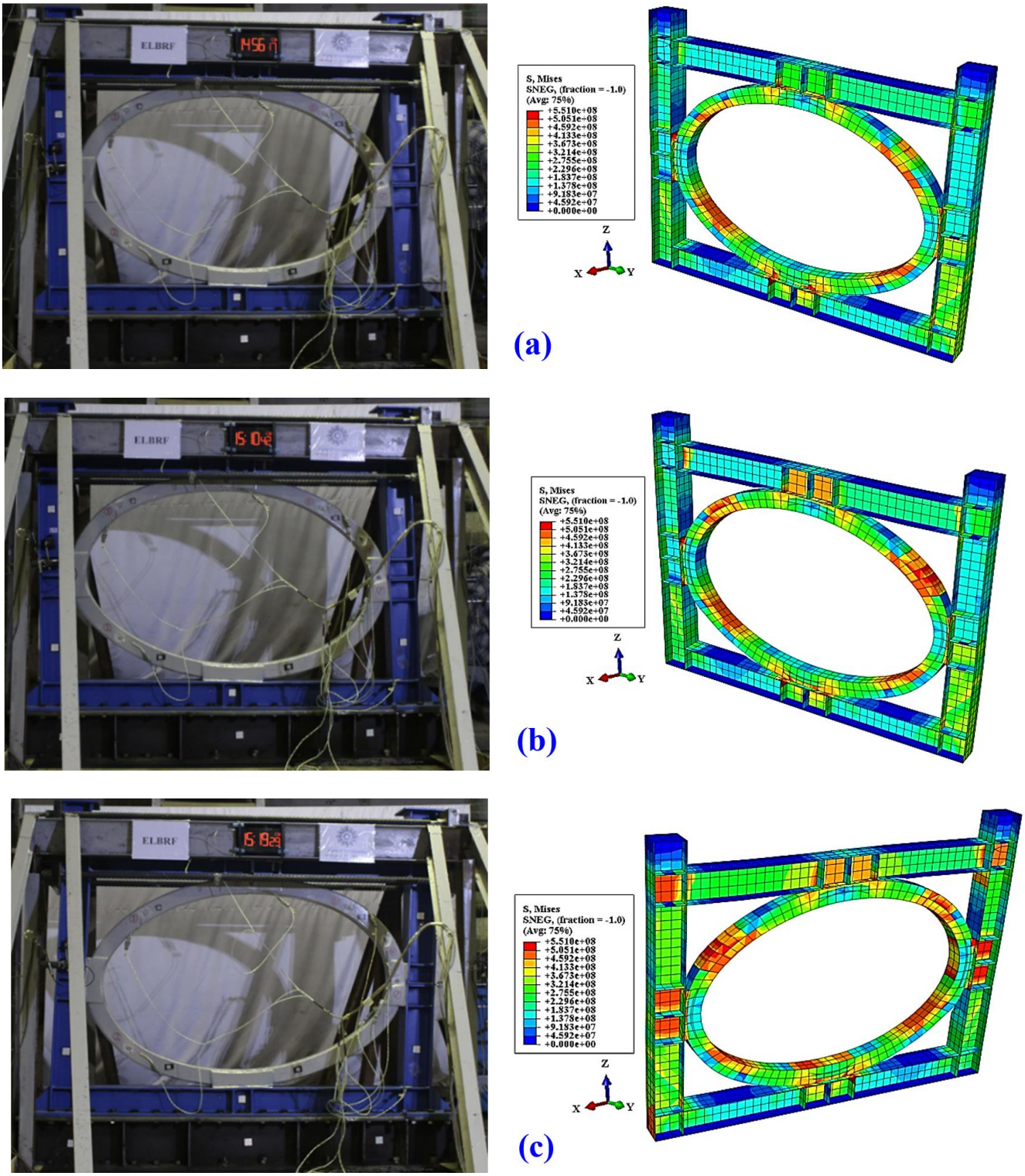

Fig. 22 The deformation and von-Mises stress (Pa) due to experimental and numerical studies in the Elliptic-braced frame (a) at 46 *mm* displacement, equal with 3.0% drift, (b) at 62 *mm* displacement, equal with 4.1% drift and (c) at 78 *mm* displacement, equal with 5.1% drift

both ends of the column, hence avoiding early destruction. With regard to the cracks, which appeared in the weld lines, the transmission path at the junction of the elliptic bracing to the beams and columns was parallel to the longitudinal axis of the borderline elements. In other words, the force transmission path of the elliptic bracing in the middle of the columns was not perpendicular to the vertical axis, and therefore, no buckling was observed in the column. From all the observations, it can be concluded that the system did not behave similarly to K-brace and diamond brace.

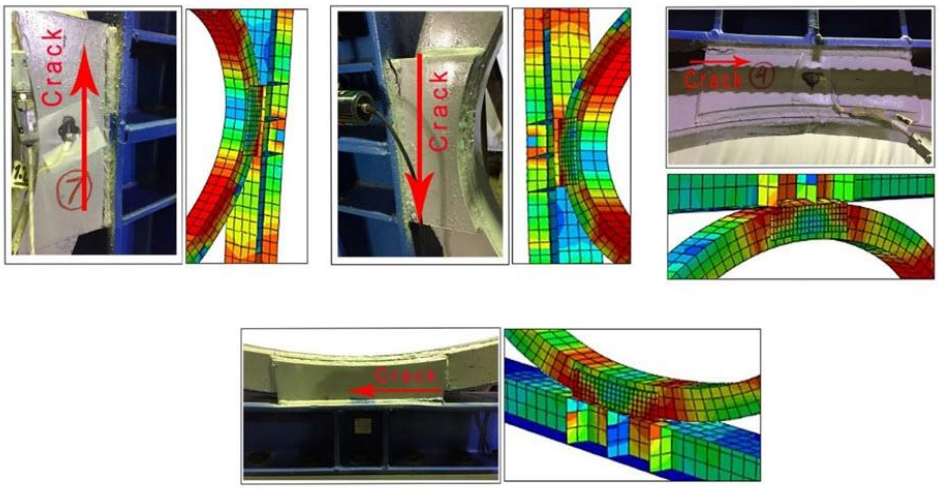

Fig. 23 The force transmission path from elliptic brace to beam and column, plastic areas at different points and cracks in the welds of the Elliptic-braced frame in test and FEM

Another significant point in this study of the proposed bracing system is that, due to the geometric shape of the elliptic brace, which is curved, in each step of the directional change in the cyclic quasi-static loading, the internal tensile forces in the members of the elliptic brace, unlike in linear braces, are quickly replaced by a compressive force.

Another merit of the curvature of elliptic brace is that by changing the direction of the lateral force, the elliptic element under pressure returns to its original state quickly and does not cause permanent deformations. Thus, no out-of-plane buckling occurs. The cyclic test results revealed that the ELBRF system had stable hysteresis loops and behaved as a lateral loading system of energy dissipation without any pinching, deterioration of stiffness, and resistance in the envelope curve. The experimental and numerical results of the behavior of the elliptic-braced frame are presented in Figs. 21 to 23.

7. Conclusions

In the current research project, an accurate method was deployed to obtain the elastic drift utilizing mathematical procedures along with structural analysis rules. For this purpose, for the first time, an equation for the elastic lateral stiffness of a two-dimensional single-story single-span EBMRF subjected to lateral force was developed. In the EBMRF, the beam-to-column connections were rigid, and the four-quarter connections of the elliptic braces were hinged to each other.

After verifying the accuracy of the proposed method to calculate the elastic lateral stiffness by conducting several finite element analyses of the EBMRF using OpenSees software, a numerical example was utilized to determine the elastic drift and elastic lateral stiffness of the EBMRF. Finally, the developed formulas were employed and equivalent stiffness for elliptic brace was developed. The most important findings are outlined below:

- For the first time to determine the actual value of elastic drift and elastic lateral stiffness of EBMRF, a developed analytical approach with simple linear formulas were proposed.
- According to the results, proper evaluation of the exact amount of elastic lateral stiffness helps to come up with an optimum design of the elastic behavior of the EBMRF system design.
- In this study, all of the effects of the deformations of the beams, columns and the elliptic brace caused by axial and shear forces and the bending moment were considered in calculating the lateral elastic stiffness of an EBMRF. There was almost a 2% error with elastic drift and lateral elastic stiffness obtained from the developed equations, which shows the accuracy of the developed equations. Moreover, the linear design equations proposed in this study are easy to use and possess enough conservative considerations.
- The proposed linear formulas are capable of calculating the elastic drift and elastic lateral stiffness of EBMRF using any type of steel profile for frame elements.
- The strain energy due to the bending moment of the elliptic brace has a greater effect on the elastic lateral stiffness of EBMRF.
- The equations proposed to calculate elastic drift and lateral elastic stiffness could be generalized for complex structures.

References

Dawe, D.J. (1974), "Curved finite element for the analysis of shallow and deep arches", *J. Comput. Struct*., **4**, 559-580. https://doi.org/10.1016/0045-7949(74)90007-8.

Dawe, D.J. (1974), "Numerical studies using circular arch finite elements", *J. Comput. Struct*., **4**, 729-740. https://doi.org/10.1016/0045-7949(74)90041-8.

Dahlberg (2004), "Procedure to calculate deflections of curved beams", *Int. J. Engng Ed*., **20**(3), 503-513.

https://doi.org/10.5923/j.jmea.20150501.02.

Fateh, A., Hejazi, F., Saleh Jaafara, M. and Bin Adnan, A. (2016), "Design of a variable stiffness bracing system: Mathematical modeling, fabrication, and dynamic analysis", *J. Soil Dyn. Earth. Eng*., **80**, 87-101. https://doi.org/10.1016/j.soildyn.2015.10.009.

Gimena, F.N., Gonzaga, P. and Gimena, L. (2008), "3D-curved beam element with varying cross-sectional area under generalized loads", *J. Eng. Struct*., **30**, 404-411. https://doi.org/10.1016/j.engstruct.2007.04.005.

Gimena, L., Gimena, F.N. and Gonzaga, P. (2008), "Structural analysis of a curved beam element defined in global coordinates", *J. Eng. Struct*., **30**, 3355-64.

Grande, E. and Rasulo, A. (2013), "Seismic assessment of concentric X-braced steel frames", *J. Eng. Struct*., **49**, 983-995. https://doi.org/10.1016/j.engstruct.2013.01.002.

Ghasemi J.H., Haghollahi A., Moghaddam H. and Sarvghad Moghadam. A.R. (2016), "Study of the seismic performance of steel frames in the elliptic bracing", *JVE Int. LTD. J. Vibro Eng*., **18**(5), 2974-2985. https://doi.org/10.21595/jve.2016.16858.

Ghasemi, J.H., Haghollahi, A., Moghaddam, H. and Sarvghad Moghadam., A.R. (2019), "Assessing seismic performance of elliptic braced moment resisting frame through pushover method", *J. Rehab. Civil Eng*., **2**, 1-17. https://doi.org/10.22075/JRCE.2018.13030.1232.

Ghasemi, J.H. and Haghollahi, A. (2020), "Assessing the seismic behavior of Steel Moment Frames equipped by elliptical brace through incremental dynamic analysis (IDA)", *J. Earth. Eng. Eng. Vib*., **19**(2), 435-449. https://doi.org/10.1007/s11803-020-0572-z.

Ghasemi, J.H. and Haghollahi, A. (2020), "Experimental study on hysteretic behavior of steel moment frame equipped with elliptical Brace", *J. Steel Comp Struct*., **34**(6), 891-907. https://doi.org/10.12989/scs.2020.34.6.891.

Ghasemi, J.H., Haghollahi, A. and Beheshti-Aval, S.B. (2020), "Experimental study of failure mechanisms in elliptic-braced steel frame", *J. Steel Comp Struct*., **37**(2), 175-191. https://doi.org/10.12989/scs.2020.37.2.175.

Ghasemi, J.H. and Haghollahi, A. (2020), "Experimental and analytical study in determining the seismic demand and performance of the ELBRF-E and ELBRF-B braced frames", *Steel Comp Struct*., **37**(5), 571-587. https://doi.org/10.12989/scs.2020.37.5.571.

Ghasemi, J.H., Haghollahi, A., Talebi Kalaleh., M. and Beheshti-Aval, S.B. (2021), "Nonlinear seismic behavior of elliptic-braced moment resisting frame using equivalent braced frame", *Steel Comp Struct*., **40**(1), 45-64. https://doi.org/10.12989/scs.2021.40.1.045 45.

Ghasemi, J.H., Haghollahi, A. and Mortazavi, M. (2022), "Pushover analysis for estimating seismic demand of elliptic braced moment resisting frames", *J. Građevinar*, **74**(11), 941-955. https://doi.org/10.14256/JCE.2311.2017.

Ghasemi, J.H., Fanaie, N., and Haghollahi, A. (2022), "Theoretical formulation for calculating elastic lateral stiffness in a simple steel frame equipped with elliptic", *Steel Compos. Struct*., **45** (3), 437-454. https://doi.org/10.12989/scs.2022.45.3.437.

Ghasemi, J.H., Haghollahi, A. and Mortazavi, M. (2022), "Analiza postupnog guranja za procjenu seizmičkih zahtjeva okvira s eliptičnim vezovima", *J. Građevinar*, **74** (11), 941-955. https://doi.org/10.14256/JCE.2311.2017.

Hadi, W.K. (2002), *Elastic Plastic Analysis of Reinforced Concrete Shallow Arched Frames Using Curved Beam Element*, Master Thesis, Department of Civil Engineering, University of Babylon-Iraq.

Haktanir, V. (1995), "The complementary functions method for the element stiffness matrix of arbitrary spatial bars of helicoidal axes", *Int J. Numer Meth Eng*., **38**, 1031-1056. https://doi.org/10.1002/nme.1620380611.

Hibbeler, R.C. (2018), *Structural Analysis*, University of Louisiana", Lafayette.

Holmes, A.M.C. (1957), "Analysis of helical beams under symmetrical loading", *J. Struct. Div*., **83**(6), 1-37. https://doi.org/10.1061/JSDEAG.0000165.

Horibe, T. and Mori, K. (2015), "In-plane and out-of-plane deflection of J-shaped beam", *J. Mech. Eng. Automation*, **5**(1), 14-19.

Just, D.J. (1982), "Circularly curved beams under plane loads", *J. Struct. Div*., **11**(8), 1858-1873. https://doi.org/10.1061/JSDEAG.0006024.

Kardestuncer, H. (1974), *Elementary Matrix Analysis of Structures*, New York: McGraw-Hill, https://doi.org/10.1016/j.engstruct.2008.05.011.

Li, X., Zhao, Y., Zhu, C. and Chen, C. (2012), "Exact solutions of stiffness matrix for curved beams with pinned – pinned ends", *J. Adv. Mater. Res*., **368-373**, 3117-3120. https://doi.org/10.4028/www.scientific.net/AMR.368-373.3117.

Litewka, P. and Rakowski, J. (1998), "The exact thick arch finite element", *J. Comput. Struct*., **68**, 369-379. https://doi.org/10.1016/S0045-7949(98)00051-0.

Love, A.E.H. (1994), *A Treatise on the Mathematical Theory of Elasticity*, New York: Dover.

MacRae, G.A., Kimura, Y. and Roeder, C. (2016), "Effect of column stiffness on braced frame seismic behavior", *J. Soil Dyn. Earth. Eng*., **80**, 87-101. https://doi.org/10.1061/(ASCE)0733-9445(2004)130:3(381).

Marquis, J.P. and Wang, T.M. (1989), "Stiffness matrix of parabolic beam element", *J. Comput Struct*., **6**, 863-870. https://doi.org/10.1016/0045-7949(89)90271-X.

Mazzoni, S., McKenna, F., Scott, M.H., Fenves, G.L. and Jeremic, B. (2013), *OpenSees Command Language Manual*.

Michalos, J.P. (1958), *Theory of Structural Analysis and Design*, New York: Ronald Press Company.

Morris, D.L. (1968), "Curved beam stiffness coefficients", *J. Struct. Div*., **94**, 1165-1178. https://doi.org/10.1061/JSDEAG.0001949.

Muhaisin, M.H. (2003), *Influence of Moving Load upon Deformations of Reinforced Concrete Frames*, Master Thesis, Department of Civil Engineering, University of Babylon-Iraq.

Palaninathan, R. and Chandrasekharan, P.S. (1958), "Curved beam stiffness coefficients", *J. Comput. Struct*., **21**, 663-669. https://doi.org/10.1061/JSDEAG.0001949.

Pan, W., Eatherton, M.R., Nie, X. and Fan, J. (2018), "Design of pre-tensioned cable-stayed buckling restrained braces considering interrelationship between bracing strength and stiffness requirements", *J. Struct. Eng*., **144**, 4018169. https://doi.org/10.1061/(ASCE)ST.1943-541X.0002162.

Pan, W.H. and Tong, J.Z. (2020), "A new stiffness-strength-relationship-based design approach for global buckling prevention of buckling-restrained braces", *J. Adv. Struct. Eng*., 1-14. https://doi.org/10.1177/1369433220974780.

Pan, W.H., Tong, J.Z., Guo, Y.L. and Wang, C.M. (2020), "Optimal design of steel buckling-restrained braces considering stiffness and strength requirements", *J. Eng. Struct*., **211**, 110437. https://doi.org/10.1016/j.engstruct.2020.110437.

Petrolo, A.S. and Casciaro, R. (2004), "3D beam element based on Saint Venànt's rod theory", *J. Comput Struct*., **82**, 2471-81. https://doi.org/10.1016/j.compstruc.2004.07.004.

Rezaiee-Pajand, M. and Rajabzadeh-Safaei, N. (2016), "An explicit stiffness matrix for parabolic beam element", *J. Latin Amer. J. Solids Struct*., **13**, 1782-1801. https://doi.org/10.1590/1679-78252820.

Sabelli, R., Mahin, S. and Chang, C. (2003), "Seismic demands on steel braced frame buildings with buckling restrained braces", *J. Eng. Struct*., **25**, 655-666. https://doi.org/10.1016/S0141-

0296(02)00175-X.
Todd, A., Helwig, M. and Joseph, A. (2008), "Shear Diaphragm Bracing of Beams. I: Stiffness and Strength Behavior". J. Struct. Eng.,134 (3), 348-356. https://doi.org/10.1061/(ASCE)07339445(2008)134:3(348).
Upadhyay, H., Rao, N. and Desai, P. (2018), "Direct stiffness method for a curved beam and analysis of a curved beam using SAP", *Interdiscipl. J. Navrachana University*, **2**(1), 1-10.
Xie, X., Xu, L. and Li, Zh. (2020), "Hysteretic model and experimental validation of a variable damping self-centering brace", *J. Construc. Steel Res*., **167**, 105965. https://doi.org/10.1016/j.jcsr.2020.105965.
Xu, L., Chen, P. and Li, Z. (2021), "Development and validation of a versatile hysteretic model for pre-compressed self-centering buckling-restrained brace", *J. Construc. Steel Res*., **177**, 106473. https://doi.org/10.1016/j.jcsr.2020.106473.
Xu, L., Lin. Z. and Xie, X. (2022), "Assembled self-centering energy dissipation braces and a force method-based model", *J. Construct. Steel Res*., **190**, 107121. https://doi.org/10.1016/j.jcsr.2021.107121.
Yamada, Y. and Ezawa, Y. (1977), "On curved finite element for the analysis of circular arches", *Int J Numer. Meth. Eng*., **4**, 1635-1651. https://doi.org/10.1002/nme.1620111102.
Yu, A.M. (2004), "Solution of the integral equations for shearing stresses in two-material curved beams", *Mech. Res. Commun*, **31**, 137-146. https://doi.org/10.1016/S0093-6413(03)00090-9.
Yu, A.M. and Nie, G.H. (2005), "Explicit solutions for shearing and radial stresses in curved beams", *J. Mech. Res. Commun*, 32, 323-331. https://doi.org/10.1016/j.mechrescom.2004.10.006.
Yu, A.M., Yang, X.G. and Nie, G.H. (2006), "Generalized coordinate for warping of naturally curved and twisted beams with general cross-sectional shapes", *Int J Solids Struct*., **43**, 2853-2867. https://doi.org/10.1016/j.ijsolstr.2005.05.045.
Yu, A.M. and Nie, G.H. (2007), "Tangential stresses in two-material curved beams", *Meccanica*, **42**, 307-311. https://doi.org/10.1007/s11012-007-9056-8.

CC

Appendix A

A.1. Strain energy of the column

Assuming infinite axial stiffness for the columns, the strain energy due to the axial forces in the elements *AE* and *DE* is zero. As demonstrated in Fig. A1, in the analysis of the internal actions of the column *AD* in the elliptic-braced steel half-frame, the amounts of the internal bending moments in the elements *AE* and *DE* are calculated by Eqs. (A-1) and (A-2).

$$M_{AE}(x) = -V_{AE}x - M_{AB} \quad , \quad 0 \le x \le \frac{L_c}{2} \tag{A1}$$

$$M_{DE}(x) = -V_{DE}x + M_{DC} \quad , \quad 0 \le x \le \frac{L_c}{2} \tag{A2}$$

The values of the strain energy due to the bending, shear and axial deformations for the column element of the elliptic-braced steel half-frame are calculated by Eqs. (A-3) and (A-4):

$$\begin{aligned} U_{AE} &= \frac{1}{2EI_c}\int_0^{\frac{L_c}{2}} M_{AE}^2(x)dx + \alpha_{s,c}\frac{V_{AE}^2 \times \left(\frac{L_c}{2}\right)}{2EA_c} + \frac{N_{AE}^2 \times \left(\frac{L_c}{2}\right)}{2EA_c} \\ &= \frac{1}{2EI_c}\int_0^{\frac{L_c}{2}} (-V_{AE}x - M_{AB})^2 dx \\ &\quad + \frac{L_c}{4EA_c}\left(\alpha_{s,c}V_{AE}^2 + N_{AE}^2\right) \\ &= \frac{1}{2EI_c}\int_0^{\frac{L_c}{2}} (V_{AE}^2x^2 + 2M_{AB}V_{AE} + M_{AB}^2)dx \\ &\quad + \frac{\left(\alpha_{s,c}V_{AE}^2 + N_{AE}^2\right)L_c}{4EA_c} \\ &= \frac{V_{AE}^2L_c^3}{48EI_c} + \frac{M_{AB}V_{AE}L_c^2}{8EI_c} + \frac{M_{AB}^2L_c}{4EI_c} \\ &\quad + \frac{\left(\alpha_{s,c}V_{AE}^2 + N_{AE}^2\right)L_c}{4EA_c} \end{aligned} \tag{A3}$$

$$\begin{aligned} U_{DE} &= \frac{1}{2EI_c}\int_0^{\frac{L_c}{2}} M_{DE}^2(x)dx + \alpha_{s,c}\frac{V_{DE}^2 \times \left(\frac{L_c}{2}\right)}{2EA_c} + \frac{N_{DE}^2 \times \left(\frac{L_c}{2}\right)}{2EA_c} \\ &= \frac{1}{2EI_c}\int_0^{\frac{L_c}{2}} (-V_{DE}x + M_{DC})^2 dx \\ &\quad + \frac{L_c}{4EA_c}\left(\alpha_{s,c}V_{DE}^2 + N_{DE}^2\right) \\ &= \frac{1}{2EI_c}\int_0^{\frac{L_c}{2}} (V_{DE}^2x^2 - 2M_{DC}.V_{DE} + M_{DC}^2)dx \\ &\quad + \frac{\left(\alpha_{s,c}V_{DE}^2 + N_{DE}^2\right)L_c}{4EA_c} \\ &= \frac{V_{DE}^2L_c^3}{48EI_c} - \frac{M_{DC}V_{DE}L_c^2}{8EI_c} + \frac{M_{DC}^2L_c}{4EI_c} \\ &\quad + \frac{\left(\alpha_{s,c}V_{DE}^2 + N_{DE}^2\right)L_c}{4EA_c} \end{aligned} \tag{A4}$$

Where U_{AE} and U_{DE} are the strain energies due to the bending deformations of the column elements *AE* and *DE*, M_{AE} and M_{DE} are the internal bending moments of the elements *AE* and *DE*, and V_{AE} and V_{DE} are the internal shear forces of the elements *AE* and *DE*, respectively. Furthermore, *E* is the elastic modulus of the utilized steel,

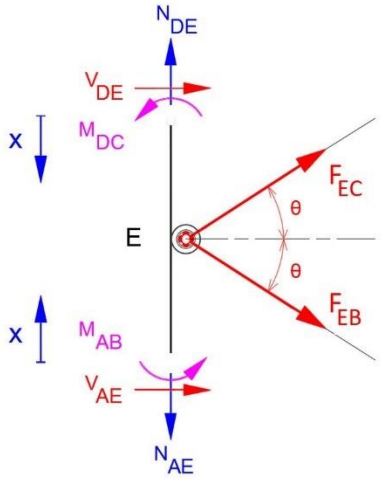

Fig. A1 The internal actions of column *AD* in the elliptic-braced steel half-frame

and I_c is the moment of inertia of the column about the bending axis (strong axis). Also, $\alpha_{s,c}$ and $\alpha_{s,b}$ are shape dependent factors for shear in beam and column elements, respectively.

Given $tan\theta = \frac{L_c}{L_b} = e$, $A_c = \frac{I_c}{r_c^2}$, incorporating Eq. (16) into Eq. (A3) and Eq. (19) into Eq. (A4) leads to the terms of Eqs. (A3) and (A4), respectively, as follows:

$$\begin{aligned} U_{AE} = &\frac{\left(\frac{P}{2} - \frac{R_C}{e} - \frac{2M_{AB}}{L_c}\right)^2 L_c^3}{48EI_c} + \frac{M_{AB}^2L_c}{4EI_c} + \\ &\left(\frac{P}{2}M_{AB} - \frac{R_C}{e}M_{AB} - \frac{2M_{AB}^2}{L_c}\right)\frac{L_c^2}{8EI_c} + \\ &\frac{\left(\alpha_{s,c}\left(\frac{P}{2} - \frac{R_C}{e} - \frac{2M_{AB}}{L_c}\right)^2 + e^2\left(P - \frac{2M_{AB}}{L_c}\right)^2\right)L_cr_c^2}{4EI_c} \end{aligned} \tag{A5}$$

$$\begin{aligned} U_{DE} = &\frac{\left(\frac{P}{2} - \frac{R_C}{e} + \frac{2M_{DC}}{L_c}\right)^2 L_c^3}{48EI_c} + \\ &\frac{M_{DC}^2L_c}{4EI_c} - \frac{L_c^2}{8EI_c}\left(\frac{P}{2}M_{DC} - \frac{R_C}{e}M_{DC} + \frac{2M_{DC}^2}{L_c}\right) + \\ &\frac{\left(\alpha_{s,c}(\frac{P}{2} - \frac{R_C}{e} + \frac{2M_{DC}}{L_c})^2 + e^2\frac{4M_{DC}^2}{L_c^2}\right)L_cr_c^2}{4EI_c} \end{aligned} \tag{A6}$$

By summing Eq. (A5) and Eq. (A6) and simplifying by$e = \frac{L_c}{L_b}$, the total value of strain energy for the column elements *AE* and *DE* due to bending, shear and axial deformations in the elliptic-braced steel half-frame is calculated as follows:

$$\begin{aligned} &U_{column} = U_{AE} + U_{DE} \\ &U_{column} = \frac{L_c}{48EI_c}\left[\left(1 + \frac{12\alpha_{s,c}r_c^2}{L_c^2}\right)\left(\frac{P}{2}L_c - R_CL_b - 2M_{AB}\right)^2\right. \\ &\quad + \\ &\left(1 + \frac{12\alpha_{s,c}r_c^2}{L_c^2}\right)\left(\frac{P}{2}L_c - R_CL_b + 2M_{DC}\right)^2 + \\ &3PL_c(M_{AB} - M_{DC}) + 6R_CL_b(M_{DC} - M_{AB}) \quad + \end{aligned} \tag{A7}$$

$$\frac{12e^2r_c^2}{L_c^2}(4M_{DC}^2-(PL_c-2M_{AB})^2)\Big]$$

A.2 Strain energy of the beams

According to the analysis of the internal forces in the elliptic-braced steel half-frame, as shown in Fig. 4, the values of the internal bending moment for the elements *AE* and *DE* are calculated by Eqs. (A8) and (A9), respectively.

$$M_{AB}(x)=-V_{AB}x+M_{AB}\quad,\quad 0\le x\le\frac{L_b}{2} \tag{A8}$$

$$M_{DC}(x)=-V_{DC}x+M_{DC}\quad,\quad 0\le x\le\frac{L_b}{2} \tag{A9}$$

The values of strain energy due to the bending, shear and axial deformations for the beam elements *AB* and *DC* of the elliptic-braced steel half-frame are calculated by Eqs. (A-10) and (A11), respectively as follows:

$$\begin{aligned}U_{AB}&=\frac{1}{2EI_b}\int_0^{\frac{L_b}{2}}M_{AB}^2(x)dx+\alpha_{s,b}\frac{V_{AB}^2\left(\frac{L_b}{2}\right)}{2EA_b}\\&\quad+\frac{N_{AB}^2\left(\frac{L_b}{2}\right)}{2EA_b}\\&=\frac{1}{2EI_b}\int_0^{\frac{L_b}{2}}(-V_{AB}x+M_{AB})^2dx\\&\quad+\frac{(\alpha_{s,b}V_{AB}^2+N_{AB}^2)L_b}{4EA_b}\\&=\frac{1}{2EI_b}\int_0^{\frac{L_b}{2}}(V_{AB}^2x^2-2M_{AB}V_{AB}+M_{AB}^2)dx\\&\quad+\frac{(\alpha_{s,b}V_{AB}^2+N_{AB}^2)L_b}{4EA_b}\\&=\frac{V_{AB}^2L_c^3}{48EI_b}-\frac{M_{AB}V_{AB}L_b^2}{8EI_b}+\frac{M_{AB}^2L_b}{4EI_b}\\&\quad+\frac{(\alpha_{s,b}V_{AB}^2+N_{AB}^2)L_b}{4EA_b}\end{aligned} \tag{A10}$$

$$\begin{aligned}&\int_0^{\frac{L_b}{2}}M_{DC}^2(x)dx+\alpha_{s,b}\frac{V_{DC}^2\left(\frac{L_b}{2}\right)}{2EA_b}+\frac{N_{DC}^2\left(\frac{L_b}{2}\right)}{2EA_b}\\&\quad=\frac{1}{2EI_b}\int_0^{\frac{L_b}{2}}(-V_{DC}x+M_{DC})^2dx\\&\qquad+\alpha_{s,b}\frac{V_{DC}^2\left(\frac{L_b}{2}\right)}{2EA_b}+\frac{N_{DC}^2\left(\frac{L_b}{2}\right)}{2EA_b}\\&\quad=\frac{1}{2EI_b}\int_0^{\frac{L_b}{2}}(V_{DC}^2x^2-2M_{DC}V_{DC}+M_{DC}^2)dx\\&\qquad+\frac{(\alpha_{s,b}V_{DC}^2+N_{DC}^2)L_b}{4EA_b}\\&\quad=\frac{V_{DC}^2L_c^3}{48EI_b}-\frac{M_{DC}V_{DC}L_b^2}{8EI_b}+\frac{M_{DC}^2L_b}{4EI_b}\\&\qquad+\frac{(\alpha_{s,b}V_{DC}^2+N_{DC}^2)L_b}{4EA_b}\end{aligned} \tag{A11}$$

Where U_{AE} and U_{DE} are the strain energies because of the bending deformations of the column elements *AE* and *DE*, M_{AE} and M_{DE} are the internal bending moments of the elements *AE* and *DE*, and V_{AE} and V_{DE} are the internal shear forces of the elements *AE* and *DE*, respectively. Also, *E* is the elastic modulus of the utilized steel, and I_c is the moment of inertia of the column about the bending axis (strong axis).

Incorporating Eq. (4) into Eq. (A10) and Eq. (3) into Eq. (A11) leads to the constituent terms of Eqs. (A10) and (A11), respectively, as follows:

$$U_{AB}=\frac{M_{AB}^2L_b}{12EI_b}+\frac{\left(\frac{4\alpha_{s,b}M_{AB}^2}{L_b^2}+\left(P-\frac{R_C}{e}-\frac{2M_{AB}}{L_be}\right)^2\right)L_b}{4EA_b} \tag{A12}$$

$$U_{DC}=\frac{M_{DC}^2L_b}{12EI_b}+\frac{\left(\frac{4\alpha_{s,b}M_{DC}^2}{L_b^2}+\left(\frac{2M_{DC}}{L_be}-\frac{R_C}{e}\right)^2\right)L_b}{4EA_b} \tag{A13}$$

By summing Eq. (A12) and Eq. (A13) and using$A_b=\frac{I_b}{r_b^2}$, the total value of strain energy for the beam elements *AB* and *DC* due to the bending, shear and axial deformations in the elliptic-braced steel half-frame is calculated as follows:

$$\begin{aligned}U_{Beams}&=U_{AB}+U_{DC}\\&=\frac{L_b}{12EI_b}\Bigg[\left(1+\frac{12\alpha_{s,b}r_b^2}{L_b^2}\right)(M_{AB}^2+M_{DC}^2)\\&=+\frac{3r_b^2}{e^2L_b^2}((PL_c-R_CL_b-2M_{AB})^2\\&\qquad+(2M_{DC}-R_CL_b)^2)\Bigg]\end{aligned} \tag{A14}$$